LETTER

doi:10.1038/nature24049

RNA targeting with CRISPR–Cas13

Omar O. Abudayyeh[1,2,3,4,5]*, Jonathan S. Gootenberg[1,2,3,4,6]*, Patrick Essletzbichler[1,2,3,4], Shuo Han[7], Julia Joung[1,2,3,4], Joseph J. Belanto[8,9], Vanessa Verdine[1,2,3,4], David B. T. Cox[1,2,3,4,10], Max J. Kellner[1], Aviv Regev[1,10], Eric S. Lander[1,6,10], Daniel F. Voytas[8,9], Alice Y. Ting[7] & Feng Zhang[1,2,3,4]

RNA has important and diverse roles in biology, but molecular tools to manipulate and measure it are limited. For example, RNA interference[1–3] can efficiently knockdown RNAs, but it is prone to off-target effects[4], and visualizing RNAs typically relies on the introduction of exogenous tags[5]. Here we demonstrate that the class 2 type VI[6,7] RNA-guided RNA-targeting CRISPR–Cas effector Cas13a[8] (previously known as C2c2) can be engineered for mammalian cell RNA knockdown and binding. After initial screening of 15 orthologues, we identified Cas13a from *Leptotrichia wadei* (LwaCas13a) as the most effective in an interference assay in *Escherichia coli*. LwaCas13a can be heterologously expressed in mammalian and plant cells for targeted knockdown of either reporter or endogenous transcripts with comparable levels of knockdown as RNA interference and improved specificity. Catalytically inactive LwaCas13a maintains targeted RNA binding activity, which we leveraged for programmable tracking of transcripts in live cells. Our results establish CRISPR–Cas13a as a flexible platform for studying RNA in mammalian cells and therapeutic development.

To achieve robust Cas13a-mediated RNA knockdown, we first evaluated 15 Cas13a orthologues for protospacer flanking site (PFS) preference and activity using a previously described ampicillin-resistance assay[8] (Fig. 1a and Extended Data Fig. 1a). This assay monitors Cas13a-mediated cleavage of the *β-lactamase* (ampicillin resistance) transcript, resulting in bacterial death under ampicillin selection, which can be measured by quantifying surviving colonies. Using this approach, we found that the Cas13a orthologue from *L. wadei* (LwaCas13a) was most active, followed by the previously characterized LshCas13a (from *Leptotrichia shahii*)[8] (Fig. 1b and Extended Data Fig. 1b). Analysis of the sequenced PFS distributions from the LwaCas13a and LshCas13a screens revealed that most LwaCas13a PFS sequences were depleted (Extended Data Fig. 1c–e). Motif analysis of the depleted PFS sequences at varying thresholds revealed the expected 3′ H motif for LshCas13a, but no significant PFS motif for LwaCas13a (Fig. 1c and Extended Data Fig. 1f, g). This observation is consistent with previous studies, which have shown that LwaCas13a is more active than LshCas13a as a nucleic-acid sensor[9]. Because of its high activity and lack of PFS in bacteria, we focused on LwaCas13a for further development.

In vitro cleavage reactions with LwaCas13a demonstrated programmable RNA cleavage with a CRISPR RNA (crRNA) encoding a 28-nucleotide (nt) spacer (shorter than the 29–30 nt length found in the native *L. wadei* CRISPR array (Extended Data Fig. 2a)). These reactions confirmed the higher cleavage efficiency of LwaCas13a over LshCas13a (Extended Data Fig. 2b, c), and revealed similar biochemical characteristics for the two enzymes (Extended Data Fig. 2d–g and Supplementary Note 1), including the ability to cleave the corresponding pre-crRNA transcript (Extended Data Fig. 2h). We also explored the crRNA constraints on LwaCas13a cleavage by truncating the spacer, finding that LwaCas13a retained *in vitro* cleavage activity with spacer lengths as short as 20 nt (Extended Data Fig. 2i). Although guide lengths less than 20 nt no longer support catalytic activity, the LwaCas13–crRNA complex may still retain binding activity, providing an opportunity for orthogonal applications with a single enzyme[10].

We next evaluated the ability of LwaCas13a to cleave transcripts in mammalian cells. We cloned mammalian codon-optimized LwaCas13a into mammalian expression vectors with msfGFP fusions on the C or N terminus and either a dual-flanking nuclear export sequence or nuclear localization sequence (NLS) and evaluated expression and localization (Fig. 1d). We found that msfGFP-fused LwaCas13a constructs expressed well and localized effectively to the cytoplasm or nucleus according to the localization sequence. To evaluate the *in vivo* cleavage activity of LwaCas13a, we developed a dual-luciferase reporter system that expressed both *Gaussia* luciferase (Gluc) and *Cypridinia* luciferase (Cluc) under different promoters on the same vector, allowing one transcript to serve as the LwaCas13a target and the other to serve as a dosing control (Fig. 1e). We then designed guides against Gluc and cloned them into a $tRNA^{Val}$ promoter-driven guide expression vector. We transfected the LwaCas13a expression vector, guide vector, and dual-luciferase construct into HEK293FT cells and measured luciferase activity 48 h after transfection. We found that LwaCas13a–msfGFP–NLS resulted in the highest levels of knockdown (75.7% for guide 1, 72.9% for guide 2), comparable to position-matched short hairpin (sh)RNA controls (78.3% for guide 1, 51.5% for guide 2) (Fig. 1f), which control for accessibility and sequence in the target region; we therefore used this design for all further knockdown experiments. We also found that knockdown is most efficient with a spacer length of 28 nt (73.8%), is dose-responsive both to the input protein and guide vector amounts, and is not sensitive to RNA polymerase III promoter choice (Extended Data Fig. 3a–d).

We next tested knockdown in HEK293FT cells of three endogenous genes: *KRAS*, *CXCR4*, and *PPIB*. We observed varying levels of knockdown; and for *KRAS* and *CXCR4*, LwaCas13a knockdown (40.4% for *PPIB*, 83.9% for *CXCR4*, 57.5% for *KRAS*) was similar to RNA interference (RNAi) with position-matched shRNAs (63.0% for *PPIB*, 73.9% for *CXCR4*, 44.3% for *KRAS*) (Fig. 1g). We also found that knockdown of *KRAS* was possible with either U6 or $tRNA^{Val}$ promoters (Extended Data Fig. 3e). Similar results were obtained in the A375 melanoma cell line (Extended Data Fig. 3f). In all cases tested, knockdown was abolished by mutating the catalytic domain of LwaCas13a (Extended Data Fig. 3g and Supplementary Note 2). To test whether LwaCas13a knockdown is efficient in plants, we targeted three rice (*Oryza sativa*) genes with three guides per transcript and co-transfected LwaCas13a and guide vectors into *O. sativa* protoplasts (Fig. 1h). After transfection, we observed

[1]Broad Institute of MIT and Harvard, Cambridge, Massachusetts 02142, USA. [2]McGovern Institute for Brain Research at MIT, Cambridge, Massachusetts 02139, USA. [3]Department of Brain and Cognitive Science, Massachusetts Institute of Technology, Cambridge, Massachusetts 02139, USA. [4]Department of Biological Engineering, Massachusetts Institute of Technology, Cambridge, Massachusetts 02139, USA. [5]Department of Health Sciences and Technology, Massachusetts Institute of Technology, Cambridge, Massachusetts 02139, USA. [6]Department of Systems Biology, Harvard Medical School, Boston, Massachusetts 02115, USA. [7]Departments of Genetics, Biology, and Chemistry, Stanford University, Stanford, California 94305, USA. [8]Department of Genetics, Cell Biology and Development, University of Minnesota, Minneapolis, Minnesota 55455, USA. [9]Center for Genome Engineering, University of Minnesota, Minneapolis, Minnesota 55455, USA. [10]Department of Biology, Massachusetts Institute of Technology, Cambridge, Massachusetts 02139, USA.
*These authors contributed equally to this work.

© 2017 Macmillan Publishers Limited, part of Springer Nature. All rights reserved.

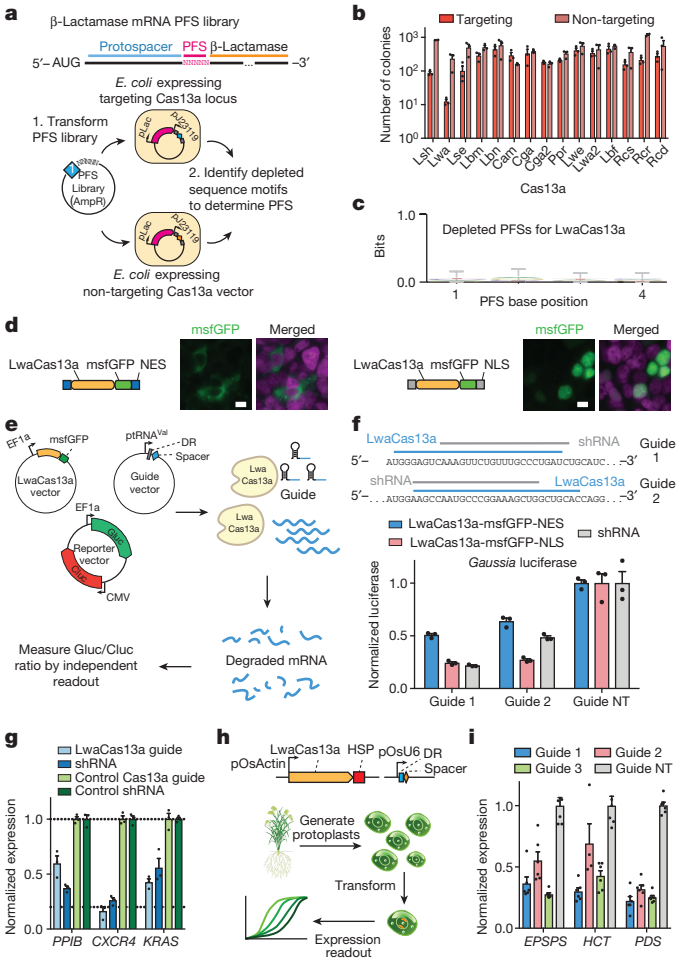

Figure 1 | Cas13a from *L. wadei* (LwaCas13a) is capable of eukaryotic transcript knockdown. a, Schematic of PFS characterization screen of Cas13a orthologues. **b**, Quantification of Cas13a activity in *E. coli* measured by colony survival from PFS screen ($n = 2$ or 3). See Extended Data Fig. 1 and Supplementary Table 10 for orthologue species used. **c**, *In vivo* PFS screening shows LwaCas13a has a minimal PFS preference. Error bars, an approximate Bayesian 95% confidence interval. **d**, Imaging showing localization and expression of each of the mammalian constructs. Scale bars, 10 μm. **e**, Schematic of the mammalian luciferase reporter system used to evaluate knockdown. DR, direct repeat. $ptRNA^{Val}$, valine tRNA promoter. **f**, Knockdown of *Gaussia* luciferase (Gluc) using engineered variants of LwaCas13a. Sequences for guides and shRNAs are shown above. NT, non-targeting guide. **g**, Knockdown of three different endogenous transcripts with LwaCas13a compared with corresponding shRNA constructs. **h**, Schematic for LwaCas13a knockdown of transcripts in rice (*Oryza sativa*) protoplasts. pOsActin, promoter of *O. sativa* actin; pOsU6, promoter of *O. sativa* U6. **i**, LwaCas13a knockdown of three transcripts in *O. sativa* protoplasts using three targeting guides per transcript ($n = 4$ or 6). All values are mean ± s.e.m. with $n = 3$, unless otherwise noted.

>50% knockdown with seven out of the nine guides and maximal knockdown of 78.0% (Fig. 1i).

To evaluate the range of efficiency of LwaCas13a knockdown, we tiled guides along the length of four transcripts: Gluc, Cluc, *KRAS*, and *PPIB* (Fig. 2a). The Gluc and Cluc tiling screens revealed guides with greater than 60% knockdown (Fig. 2b, c), with the majority of Gluc-targeting guides exhibiting >50% knockdown and up to 83% knockdown. To compare LwaCas13a knockdown with RNAi, we selected the top three performing guides against Gluc and Cluc and compared them to position-matched shRNAs. We found that five out of six top performing guides achieved significantly higher levels of knockdown ($P < 0.05$) than their matched shRNAs (Extended Data Fig. 3h).

For endogenous genes, we found that, while knockdown efficiency was transcript dependent, there was maximal knockdown of 85% and 75% for *KRAS* and *PPIB*, respectively (Fig. 2d, e). We selected the top three guides from the *KRAS* and *PPIB* tiling screens and observed robust knockdown with LwaCas13a (53.7–88.8%) equivalent to levels attained by shRNA knockdown (61.8–95.2%), with shRNA significantly better for two out of six guides ($P < 0.01$) and LwaCas13a significantly better for two out of six guides ($P < 0.01$) (Fig. 2f). LwaCas13a can also mediate significant knockdown of the nuclear transcripts *MALAT1* and *XIST*[11], whereas position-matched shRNAs showed no detectable knockdown ($P > 0.05$) (Fig. 2g, h and Extended Data Fig. 3i)

LshCas13a activity is governed by target accessibility in *E. coli*[8], and we therefore used our data from the four tiling screens to investigate whether LwaCas13a activity is higher for guides located in regions of accessibility. We found that the most effective guides were closer together than expected by chance (Extended Data Fig. 4a), and predicted target accessibility could explain some of the variation in targeting efficacy (4.4–16% of the variation in knockdown) (Extended Data Fig. 4b–d and Supplementary Note 3).

Because LwaCas13a can process its own pre-crRNA[12], it offers the possibility of streamlined multiplexed delivery of LwaCas13a guides[13]. We designed five different guides against the endogenous *PPIB*, *CXCR4*, *KRAS*, *TINCR*, and *PCAT* transcripts and delivered the targeting system as a CRISPR array with 28-nt guides flanked by 36-nt direct repeats (representing an unprocessed direct repeat and a truncated spacer), under expression of the U6 promoter. We found levels of knockdown for each gene that were comparable to single or pooled guide controls (Fig. 2i). To evaluate specificity in this context, we tested multiplexed delivery of three guides against *PPIB*, *CXCR4*, and *KRAS* or three variants where each one of the three guides was replaced with a non-targeting guide. We found that in each case where a guide was absent from the array, only the targeted transcripts were reduced (Fig. 2j).

To further investigate the specificity of LwaCas13a *in vivo*, we introduced single mismatches into guides targeting either Gluc (Fig. 3a) or endogenous genes (Fig. 3b and Extended Data Fig. 5a, b), as well as double mismatches (Fig. 3c and Extended Data Fig. 5c), and found that knockdown was sensitive to mismatches in the central seed region of the guide–target duplex, which we additionally confirmed by biochemical profiling (Extended Data Fig. 5d–k and Supplementary Note 4). To comprehensively search for off-target effects of LwaCas13a knockdown, we performed transcriptome-wide mRNA sequencing. We targeted the Gluc transcript with LwaCas13a or a position-matched shRNA construct, and found significant knockdown of the target transcript ($P < 0.01$) (Fig. 3d, e). Similar results were found for the same comparison when targeting *KRAS* and *PPIB* ($P < 0.05$) (Extended Data Fig. 6a, b). Differential expression analysis indicated hundreds of significant off-targets in each of the shRNA conditions but none in LwaCas13a conditions (Fig. 3f), despite comparable levels of knockdown of the target transcripts (30.5%, 43.5%, and 64.7% for shRNA, 62.6%, 27.1%, and 29.2% for LwaCas13a, for Gluc, *KRAS*, and *PPIB*, respectively) (Fig. 3g). Additional analysis of the Gluc-targeting RNA-seq comparisons suggested the shRNA libraries show higher variability between targeting and non-targeting conditions compared with LwaCas13a because of these off-target effects (Extended Data Figs 6c–f and 7 and Supplementary Note 5).

The collateral activity of LshCas13a has been directly observed biochemically *in vitro* and indirectly observed through growth suppression in bacteria[8], but the extent of this activity in mammalian cells is unclear. The multiplexed leave-one-out and RNA-sequencing (RNA-seq) analyses suggested a lack of collateral RNA degradation. We verified this hypothesis by re-analysing the knockdown tiling screens (Fig. 2b–e), finding that expression of the control gene did not correlate with the expression of the targeted gene (Gluc: $R = -0.078$, $P > 0.05$; *PPIB*: $R = -0.058$, $P > 0.05$; *KRAS*: $R = -0.51$, $P < 0.001$) (Extended Data Fig. 8a–h). Additionally, in the RNA-seq experiments there were no differentially expressed genes other than the

© 2017 Macmillan Publishers Limited, part of Springer Nature. All rights reserved.

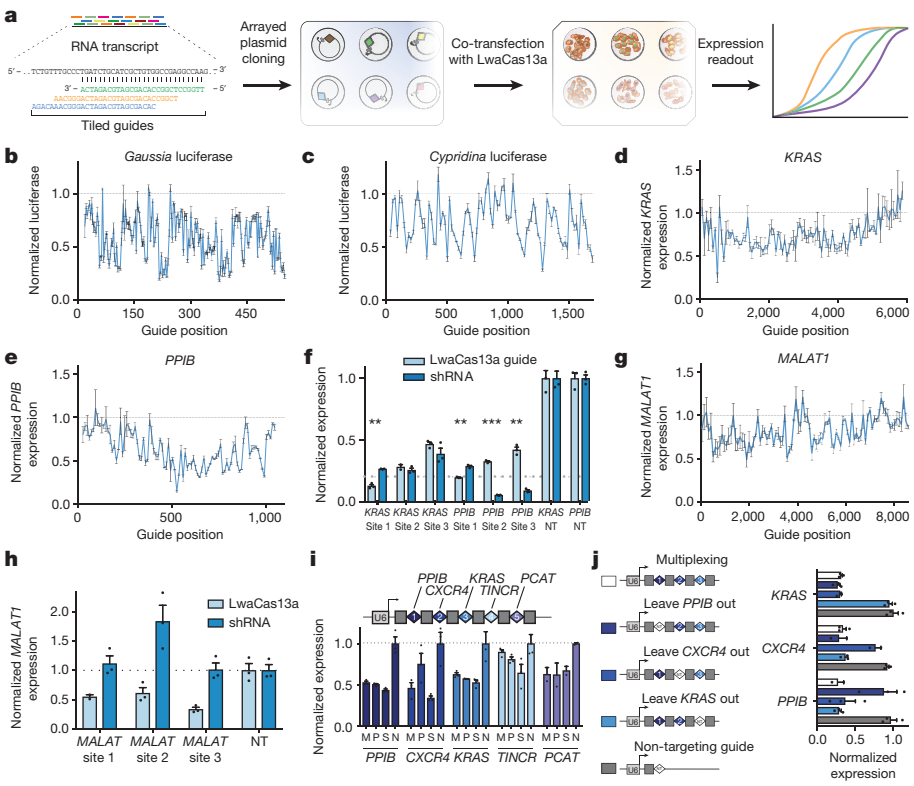

Figure 2 | LwaCas13a arrayed screening of mammalian coding and non-coding RNA targets and multiplexed guide delivery. **a**, Schematic of LwaCas13a arrayed screening. **b**–**e**, Arrayed knockdown screen of 186 guides evenly tiled across the Gluc transcript (**b**) or 93 guides evenly tiled across each of the Cluc (**c**), *KRAS* (**d**), and *PPIB* (**e**) transcripts. **f**, Validation of the top three guides from the endogenous arrayed knockdown screens with shRNA comparisons ($n = 2$ or 3) (***$P < 0.001$; **$P < 0.01$; two-tailed Student's *t*-test). NT, non-targeting guide. **g**, Arrayed knockdown screen of 93 guides evenly tiled across the *MALAT1* transcript. **h**, Validation of top three guides from the endogenous arrayed *MALAT1* knockdown screen with shRNA comparisons ($n = 2$ or 3). **i**, Multiplexed knockdown of five endogenous genes through delivery of five guides in a CRISPR array under the expression of a single promoter ($n = 2$ or 3). M, multiplexed array delivery; P, pooled single-guide delivery; S, single guide; N, non-targeting guide. **j**, Three-guide arrays containing combinations of targeting and non-targeting spacers showing sequence-specific multiplexed knockdown ($n = 2$ or 3). All values are mean ± s.e.m. with $n = 3$ (n represents the number of transfection replicates), unless otherwise noted.

target gene, indicating that LwaCas13a targeting does not lead to an observable cell stress response at the transcriptomic level[14] (Fig. 3d, e and Extended Data Fig. 6a, b), as would be reasonably expected if substantial collateral activity occurred. Furthermore, LwaCas13a-mediated knockdown of targeted transcripts did not affect the growth of mammalian cells expressing similar levels of LwaCas13a (Fig. 3h). Finally, because activation of non-specific RNA nucleases in mammalian cells results in detectable changes in RNA size distribution[15], we examined global RNA degradation in cells after LwaCas13a knockdown of Gluc transcripts and found no difference in the RNA integrity between targeting and non-targeting conditions ($P > 0.05$) (Extended Data Fig. 8i, j and Supplementary Note 6).

To expand the utility of LwaCas13a as a tool for studying RNA, we created a catalytically dead variant (dLwaCas13a) by mutating catalytic arginine residues. We quantified RNA binding by dLwaCas13a with RNA immunoprecipitation (Fig. 4a) using guides containing the

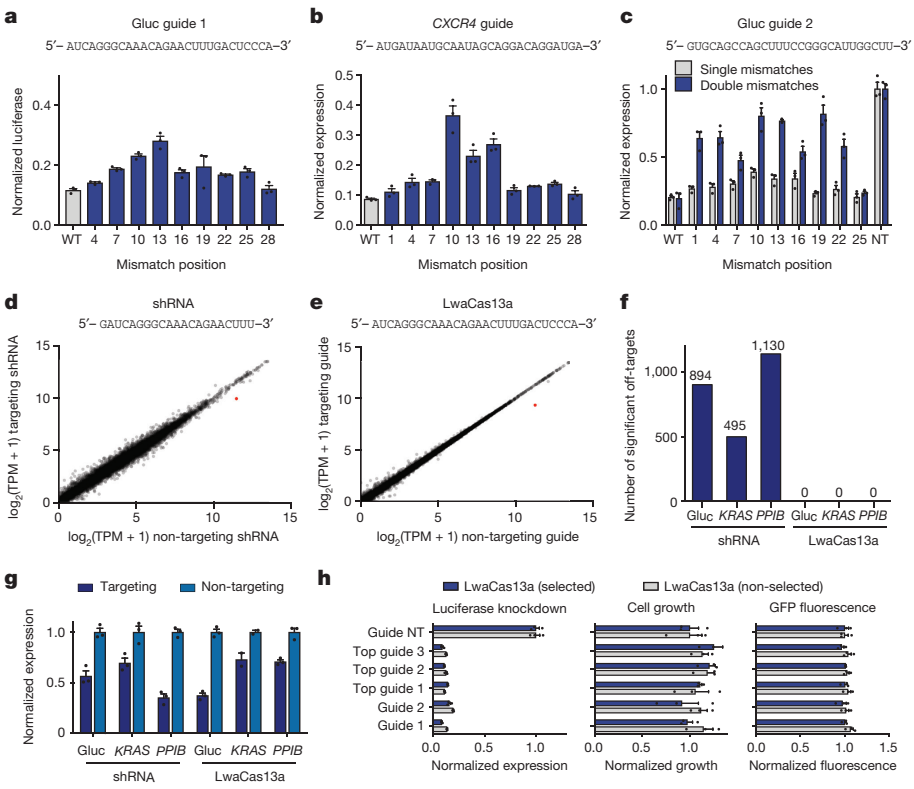

Figure 3 | Evaluation of LwaCas13a knockdown specificity and comparisons to RNA interference. **a**, **b**, Knockdown of Gluc (**a**) or *CXCR4* (**b**) evaluated with guides containing single mismatches at varying positions across the spacer sequence (shown above). WT, wild type. **c**, Knockdown of Gluc evaluated with guide 2 containing single or double mismatches at varying positions across the spacer sequence (shown above). **d**, **e**, Expression levels in $\log_2$(transcripts per million (TPM + 1)) values of all genes detected in RNA-seq libraries of non-targeting control (*x* axis) compared with Gluc-targeting condition (*y* axis) for shRNA (**d**) and LwaCas13a (**e**). Shown is the mean of three biological replicates. The Gluc transcript data point is coloured in red. The guide sequence used is shown above. **f**, Differential gene expression analysis of six RNA-seq libraries (each with three biological replicates) comparing LwaCas13a knockdown with shRNA knockdown at three different genes ($n = 2$ or 3). **g**, Quantified mean knockdown levels for the targeted genes from the RNA-seq libraries. **h**, Luciferase knockdown (left), cell viability (middle), and LwaCas13a–GFP expression (right) for cells transfected with LwaCas13a for 72 h with and without selection. All values are mean ± s.e.m. with $n = 3$ (n represents the number of transfection replicates), unless otherwise noted.

© 2017 Macmillan Publishers Limited, part of Springer Nature. All rights reserved.

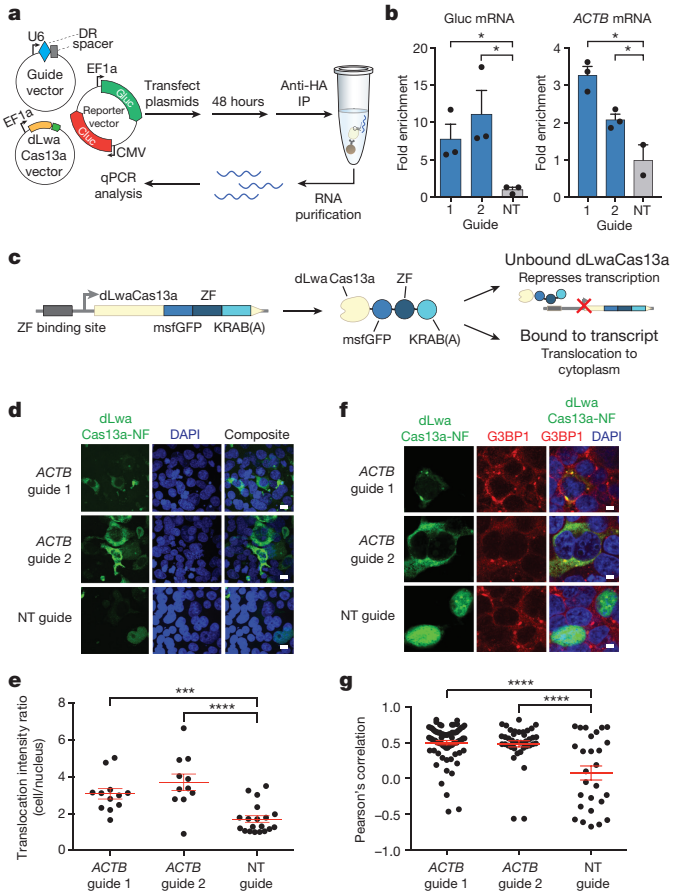

Figure 4 | Catalytically inactive LwaCas13a (dLwaCas13a) is capable of binding transcripts and tracking stress granule formation. a, Schematic of RNA immunoprecipitation for quantification of dLwaCas13a binding. **b**, dLwaCas13a targeting Gluc and *ACTB* transcripts is significantly enriched compared with non-targeting controls; $n = 2$ or 3 (n represents the number of transfection replicates). **c**, Schematic of dLwaCas13a-GFP–KRAB negative-feedback (dLwaCas13a-NF) construct used for imaging. **d**, Representative images for dLwaCas13a-NF imaging with multiple guides targeting *ACTB*. Scale bars, 10 μm. **e**, Quantification of translocation of dLwaCas13a-NF; $n = 12$, 11, and 19 (guides 1, 2, and NT) (n represents the number of individual cells analysed). **f**, Representative immunofluorescence images of HEK293FT cells treated with 400 μM sodium arsenite. Stress granules are indicated by G3BP1 staining. Scale bars, 5 μm. **g**, G3BP1 and dLwaCas13a-NF co-localization quantified per cell by Pearson's correlation. $n = 75$, 40, and 27 (guides 1, 2, and NT) (n represents the number of individual cells analysed). All values are mean ± s.e.m. $^{****}P < 0.0001$; $^{***}P < 0.001$; $^{*}P < 0.05$. A one-tailed Student's t-test was used for comparisons in **b** and a two-tailed Student's t-test was used for comparisons in **e** and **g**.

36-nt direct repeats and 28-nt spacers. We found that pulldown of dLwaCas13a targeted to either luciferase transcripts or *ACTB* mRNA (Fig. 4b) resulted in significant enrichment of the corresponding target over non-targeting controls (7.8–11.2× enrichment for luciferase and 2.1–3.3× enrichment for *ACTB*; $P < 0.05$), validating dLwaCas13a as a reprogrammable RNA binding protein.

One application for dLwaCas13a is as a transcript imaging platform. To reduce background noise due to unbound protein, we incorporated a negative-feedback (NF) system based upon zinc finger self-targeting and KRAB domain repression[16] (Fig. 4c and Supplementary Note 7). Compared with dLwaCas13a, dLwaCas13a–NF effectively translocated from the nucleus to the cytoplasm when targeted to *ACTB* mRNA (Extended Data Fig. 9a). To further characterize translocation of dLwaCas13a–NF, we targeted *ACTB* transcripts with two guides and found that both guides increased translocation compared with a non-targeting guide (3.1–3.7× cellular/nuclear signal ratio; $P < 0.001$) (Fig. 4d, e and Extended Data Fig. 9b–d). To validate dLwaCas13a–NF imaging, we analysed the correlation of dLwaCas13a–NF signal to *ACTB* mRNA fluorescent *in situ* hybridization (FISH) signal (Extended Data Fig. 10a) and found that there was significant correlation and signal overlap for the targeting guides versus the non-targeting guide conditions ($R = 0.27$ and 0.30 for guide 1 and 2, respectively, and $R = 0.00$ for the non-targeting guide condition; $P < 0.0001$) (Extended Data Fig. 10b).

Using dLwaCas13a–NF, we investigated the accumulation of mRNA into stress granules[17,18] by combining transcript imaging with visualization of stress granules marker G3BP1 (ref. 19). In fixed samples, we found significant correlations between dLwaCas13a–NF fluorescence and G3BP1 levels for *ACTB*-targeting guides compared with non-targeting controls ($R = 0.49$ and 0.50 for guide 1 and guide 2, respectively, and $R = 0.08$ for the non-targeting guide; $P < 0.001$) (Fig. 4f, g). We next performed stress granule tracking in live cells and found that dLwaCas13a–NF targeted to *ACTB* localized to significantly more stress granules per cell over time than the corresponding non-targeting control ($P < 0.05$) (Extended Data Fig. 10c, d and Supplementary Note 7).

These results show that LwaCas13a can be reprogrammed with guide RNAs to effectively knockdown or bind transcripts in mammalian cells. LwaCas13a knockdown is comparable to RNAi knockdown efficiency, but with substantially reduced off-targets, making it potentially well-suited for therapeutic applications. Furthermore, it can mediate nuclear RNA and multiplexed knockdown. Catalytically inactive dLwaCas13a can be used as a programmable RNA binding protein, which we adapted for live imaging transcript tracking. We anticipate that there will be additional applications for LwaCas13a and dLwaCas13a, such as genome-wide pooled knockdown screening, interrogation of lncRNA and nascent transcript function, pulldown assays to study RNA–protein interactions, translational modulation, and RNA base editing. Importantly, we do not observe any evidence for collateral activity of LwaCas13a in mammalian cells (Supplementary Note 6). Our data show LwaCas13a functions in mammalian and plant cells with broad efficacy and high specificity, providing a platform for a range of transcriptome analysis tools and therapeutic approaches.

Online Content Methods, along with any additional Extended Data display items and Source Data, are available in the online version of the paper; references unique to these sections appear only in the online paper.

Received 18 April; accepted 1 September 2017.
Published online 4 October 2017.

1. Fire, A. *et al.* Potent and specific genetic interference by double-stranded RNA in *Caenorhabditis elegans*. *Nature* **391,** 806–811 (1998).
2. Elbashir, S. M. *et al.* Duplexes of 21-nucleotide RNAs mediate RNA interference in cultured mammalian cells. *Nature* **411,** 494–498 (2001).
3. Root, D. E., Hacohen, N., Hahn, W. C., Lander, E. S. & Sabatini, D. M. Genome-scale loss-of-function screening with a lentiviral RNAi library. *Nat. Methods* **3,** 715–719 (2006).
4. Jackson, A. L. *et al.* Expression profiling reveals off-target gene regulation by RNAi. *Nat. Biotechnol.* **21,** 635–637 (2003).
5. Tyagi, S. Imaging intracellular RNA distribution and dynamics in living cells. *Nat. Methods* **6,** 331–338 (2009).
6. Shmakov, S. *et al.* Diversity and evolution of class 2 CRISPR–Cas systems. *Nat. Rev. Microbiol.* **15,** 169–182 (2017).
7. Shmakov, S. *et al.* Discovery and functional characterization of diverse class 2 CRISPR–Cas systems. *Mol. Cell* **60,** 385–397 (2015).
8. Abudayyeh, O. O. *et al.* C2c2 is a single-component programmable RNA-guided RNA-targeting CRISPR effector. *Science* **353,** aaf5573 (2016).
9. Gootenberg, J. S. *et al.* Nucleic acid detection with CRISPR–Cas13a/C2c2. *Science* **356,** 438–442 (2017).
10. Dahlman, J. E. *et al.* Orthogonal gene knockout and activation with a catalytically active Cas9 nuclease. *Nat. Biotechnol.* **33,** 1159–1161 (2015).
11. Hutchinson, J. N. *et al.* A screen for nuclear transcripts identifies two linked noncoding RNAs associated with SC35 splicing domains. *BMC Genomics* **8,** 39 (2007).
12. East-Seletsky, A. *et al.* Two distinct RNase activities of CRISPR–C2c2 enable guide-RNA processing and RNA detection. *Nature* **538,** 270–273 (2016).

© 2017 Macmillan Publishers Limited, part of Springer Nature. All rights reserved.

13. Zetsche, B. *et al.* Multiplex gene editing by CRISPR–Cpf1 using a single crRNA array. *Nat. Biotechnol.* **35,** 31–34 (2017).
14. Subramanian, A. *et al.* Gene set enrichment analysis: a knowledge-based approach for interpreting genome-wide expression profiles. *Proc. Natl Acad. Sci. USA* **102,** 15545–15550 (2005).
15. Rath, S. *et al.* Human RNase L tunes gene expression by selectively destabilizing the microRNA-regulated transcriptome. *Proc. Natl Acad. Sci. USA* **112,** 15916–15921 (2015).
16. Gross, G. G. *et al.* Recombinant probes for visualizing endogenous synaptic proteins in living neurons. *Neuron* **78,** 971–985 (2013).
17. Unsworth, H., Raguz, S., Edwards, H. J., Higgins, C. F. & Yagüe, E. mRNA escape from stress granule sequestration is dictated by localization to the endoplasmic reticulum. *FASEB J.* **24,** 3370–3380 (2010).
18. Nelles, D. A. *et al.* Programmable RNA tracking in live cells with CRISPR/Cas9. *Cell* **165,** 488–496 (2016).
19. Tourrière, H. *et al.* The RasGAP-associated endoribonuclease G3BP assembles stress granules. *J. Cell Biol.* **160,** 823–831 (2003).

Supplementary Information is available in the online version of the paper.

Acknowledgements We thank M. Alimova, D. Feldman, F. Chen, J. G. Doench, J. M. Engreitz, N. Habib, D. Tenen, A. Allen, R. Macrae, and R. Belliveau for discussions and support. O.A.A. is supported by a Paul and Daisy Soros Fellowship and a National Defense Science and Engineering Fellowship. J.S.G. is supported by a D.O.E. Computational Science Graduate Fellowship. A.R. is supported by the Howard Hughes Medical Institute. F.Z. is a New York Stem Cell Foundation-Robertson Investigator. F.Z. is supported by the National Institutes of Health through the National Institute of Mental Health (5DP1-MH100706 and 1R01-MH110049), the Howard Hughes Medical Institute, the New York Stem Cell, Simons, Paul G. Allen Family, and Vallee Foundations; and James and Patricia Poitras, Robert Metcalfe, and David Cheng.

Author Contributions O.O.A., J.S.G., and F.Z. conceived and designed the study. O.O.A. and J.S.G. participated in the design and execution of all experiments. P.E. performed biochemical characterization studies on the LwaCas13a protein. J.J. and V.V. prepared the vectors for arrayed knockdown screening experiments. J.J. also performed RNA immunoprecipitation experiments. D.B.T.C. assisted with cloning of constructs. M.J.K. performed the RNA integrity analysis. O.O.A. and J.S.G. analysed data. S.H. performed select microscopy experiments. J.J.B. performed the plant protoplast knockdown experiments. O.O.A., J.S.G., E.S.L., and F.Z. wrote the paper with input from D.F.V., A.Y.T., and A.R. and help from all authors.

Author Information Reprints and permissions information is available at www.nature.com/reprints. The authors declare competing financial interests: details are available in the online version of the paper. Readers are welcome to comment on the online version of the paper. Publisher's note: Springer Nature remains neutral with regard to jurisdictional claims in published maps and institutional affiliations. Correspondence and requests for materials should be addressed to F.Z. (zhang@broadinstitute.org).

© 2017 Macmillan Publishers Limited, part of Springer Nature. All rights reserved.

METHODS

No statistical methods were used to predetermine sample size. The experiments were not randomized. The investigators were not blinded to allocation during experiments and outcome assessment.

Cloning of orthologues for activity screen and recombinant expression. We synthesized human codon-optimized versions of 15 Cas13a orthologues (Genscript) (Supplementary Table 10) and cloned them into pACYC184 under a pLac promoter. Adjacent to the Cas13a expression cassette, we cloned the orthologue's corresponding direct repeats flanking either a *β-lactamase*-targeting or non-targeting spacer. Spacer array expression was driven by the J23119 promoter.

For purification of LwaCas13a, we cloned the mammalian codon-optimized LwaCas13a sequence into a bacterial expression vector for protein purification (6× His/Twin Strep SUMO, a pET-based expression vector received as a gift from I. Finkelstein, University of Texas-Austin).

All plasmids used in this study are listed in Supplementary Table 2. Information on Cas13a orthologues used in this study can be found in Supplementary Table 10.

Bacterial *in vivo* testing for Cas13a activity and PFS identity. In brief, Cas13a was programmed to target a 5′ stretch of sequence on the *β-lactamase* transcript flanked by randomized PFS nucleotides. Cas13a cleavage activity resulted in death of bacteria under ampicillin selection, and PFS depletion was subsequently analysed by next-generation sequencing.

To test for activity of Cas13a orthologues, 90 ng of orthologue expression plasmid with either targeting or non-targeting guide was co-transformed with 25 ng of a previously described β-lactamase target plasmid[8] into NovaBlue Singles Competent Cells (Millipore). Post-transformation, cells were diluted, plated on LB-agar supplemented with 100 $\mu g\,\mu l^{-1}$ ampicillin and 25 $\mu g\,\mu l^{-1}$ chloramphenicol, and incubated at 37 °C overnight. Transformants were counted the next day.

For determination of LshCas13a and LwaCas13a PFS identity, 40 ng of orthologue expression plasmid with either targeting or non-targeting spacer was co-transformed with 25 ng of β-lactamase target plasmid into two aliquots of NovaBlue GigaSingles (Millipore) per biological replicate. Two biological replicates were performed. Post-transformation, cells were recovered at 37 °C in 500 µl of SOC (ThermoFisher Scientific) per biological replicate for 1 h, plated on bio-assay plates (Corning) with LB-agar (Affymetrix) supplemented with 100 $\mu g\,\mu l^{-1}$ ampicillin and 25 $\mu g\,\mu l^{-1}$ chloramphenicol, and incubated at 37 °C for 16 h. Colonies were then harvested by scraping, and plasmid DNA was purified with NucleoBond Xtra EF (Macherey-Nagel) for subsequent sequencing.

Harvested plasmid samples were prepared for next-generation sequencing by PCR with barcoding primers and Illumina flow cell handles using NEBNext High Fidelity 2X Master Mix (New England Biosciences). PCR products were pooled and gel extracted using a Zymoclean gel extraction kit (Zymo Research) and sequenced using a MiSeq next-generation sequencing machine (Illumina).

Computational analysis of PFS. From next-generation sequencing of the LshCas13a and LwaCas13a PFS screening libraries, we aligned the sequences flanking the randomized PFS region and extracted the PFS identities. We collapsed PFS identities to four nucleotides to improve sequence coverage, counted the frequency of each unique PFS, and normalized to total read count for each library with a pseudocount of 1. Enrichment of each distribution as displayed in Extended Data Fig. 1c was calculated against the pACYC184 control (no protein/guide locus) as $-\log_2(f_{\text{condition}}/f_{\text{pACYC184}})$, where $f_{\text{condition}}$ is the frequency of PFS identities in the experimental condition and f_{pACYC184} is the frequency of PFS identities in the pACYC184 control. To analyse a conserved PFS motif, top depleted PFS identities were calculated using each condition's non-targeting control as follows: $-\log_2(f_{i,\text{targeting}}/f_{i,\text{non-targeting}})$ where $f_{i,\text{targeting}}$ is the frequency of PFS identities in condition i with targeting spacer and $f_{i,\text{non-targeting}}$ is the frequency of PFS identities in condition i with non-targeting spacer. PFS motifs were analysed for a range of thresholds as shown in Extended Data Fig. 1d, f, g.

Purification of LwaCas13a. Purification of LwaCas13a was performed as previously described[9]. In brief, LwaCas13a bacterial expression vectors were transformed into Rosetta 2(DE3)pLysS singles Competent Cells (Millipore) and 4 l of Terrific Broth 4 growth media were seeded with a starter culture. Cell protein expression was induced with IPTG and after overnight growth, the cell pellet was harvested and stored at −80 °C. Following cell lysis, protein was bound using a StrepTactin Sepharose resin (GE) and protein was eluted by SUMO protease digestion (ThermoFisher). Protein was further purified by cation exchange using a HiTrap SP HP cation exchange column (GE Healthcare Life Sciences) and subsequently by gel filtration using a Superdex 200 Increase 10/300 GL column (GE Healthcare Life Sciences), both steps via FPLC (AKTA PURE, GE Healthcare Life Sciences). Final fractions containing LwaCas13a protein were pooled and concentrated into Storage Buffer (600 mM NaCl, 50 mM Tris-HCl pH 7.5, 5% glycerol, 2 mM DTT) and aliquots were frozen at −80 °C for long-term storage.

Cloning of mammalian and plant expression constructs. The human codon-optimized *Cas13a* gene was synthesized (Genscript) and cloned into a mammalian expression vector with either a nuclear export sequence or NLS under expression of the EF1-α promoter. Because of the stability conferred by monomeric-super-folded GFP (msfGFP), we fused msfGFP to the C terminus of LwaCas13a. The full-length direct repeat of LwaCas13a was used for cloning the guide backbone plasmid with expression under a U6 promoter. The catalytically inactive LwaCas13a–msfGFP construct (dead LwaCas13a or dLwaCas13a) was generated by introducing R474A and R1046A mutations in the two HEPN domains. A drug-selectable version of LwaCas13a–msfGFP was generated by cloning the protein into a backbone with the Blasticidin selection marker linked to the C terminus via a 2A peptide sequence. The negative-feedback version of the dLwaCas13a–msfGFP construct (dLwaCas13a–NF) was generated by cloning a zinc-finger binding site upstream of the promoter of dLwaCas13a–msfGFP and fusing a zinc finger and KRAB domain to the C terminus.

The reporter luciferase construct was generated by cloning *Cypridinia* luciferase (Cluc) under expression of the CMV promoter and *Gaussia* luciferase (Gluc) under expression of the EF1-α promoter, both on a single vector. Expression of both luciferases on a single vector allowed one luciferase to serve as a dosing control for normalization of knockdown of the other luciferase, controlling for variation due to transfection conditions.

For the endogenous knockdown experiments in Fig. 1g, guides and shRNAs were designed using the RNAxs siRNA design algorithm[20]. The prediction tool was used to design shRNAs, and guides were designed in the same location to allow for comparison between shRNA and LwaCas13a knockdown.

For the plant knockdown experiments, the rice actin promoter (*pOsActin*) was PCR amplified from pANIC6A[21] and LwaCas13a was PCR amplified from human expression LwaCas13a constructs. These fragments were ligated into existing plant expression plasmids such that LwaCas13a was driven by the rice actin promoter and transcription was terminated by the HSP terminator while the LwaCas13a gRNAs were expressed from the rice U6 promoter (*pOsU6*).

All guides and shRNAs used in this study are listed in Supplementary Tables 1 and 3.

Protoplast preparation. Green rice protoplasts (*O. sativa* L. ssp. *japonica* var. Nipponbare) were prepared as previously described[22] with slight modifications. Seedlings were grown for 14 days and protoplasts were resuspended in mMG buffer containing 0.1 M $CaCl_2$. This modified mMG buffer was used to prepare fresh 40% PEG buffer as well as in place of WI buffer. Finally, protoplasts were kept in total darkness for 48 h post-transformation. All other conditions were as previously described.

Nucleic-acid target and crRNA preparation for *in vitro* reactions and collateral activity assays. To generate nucleic-acid targets, oligonucleotides were PCR amplified with KAPA Hifi Hot Start (Kapa Biosystems). dsDNA amplicons were gel extracted and purified using a MinElute gel extraction kit (Qiagen). The resulting purified dsDNA was transcribed via overnight incubation at 30 °C with a HiScribe T7 Quick High Yield RNA Synthesis kit (New England Biolabs). Transcribed RNA was purified using a MEGAclear Transcription Clean-up kit (Thermo Fisher). All RNA targets used in this study are listed in Supplementary Tables 4 and 6.

To generate crRNAs, oligonucleotides were ordered as DNA (Integrated DNA Technologies) with an additional 5′ T7 promoter sequence. crRNA template DNA was annealed with a T7 primer (final concentrations 10 µM) and transcribed via overnight incubation at 37 °C with a HiScribe T7 Quick High Yield RNA Synthesis kit (New England Biolabs). The resulting transcribed crRNAs were purified with RNAXP clean beads (Beckman Coulter), using a 2× ratio of beads to reaction volume, supplemented with additional 1.8× ratio of isopropanol (Sigma). crRNA constructs used for *in vitro* experiments are listed in Supplementary Table 5 and crRNA constructs used for collateral detection are listed in Supplementary Table 6.

LwaCas13a cleavage and collateral activity detection. For biochemical characterization of LwaCas13a, assays were performed as previously described[8]. In brief, nuclease assays were performed with 160 nM of end-labelled single-stranded (ss)RNA target, 200 nM purified LwaCas13a, and 100 nM crRNA, unless otherwise indicated. All assays were performed in nuclease assay buffer (40 mM Tris-HCl, 60 mM NaCl, 6 mM $MgCl_2$, pH 7.3). For array processing, 100 ng of *in vitro* transcribed array was used per nuclease assay. Reactions were allowed to proceed for 1 h at 37 °C (unless otherwise indicated) and were then quenched with proteinase buffer (150 U ml^{-1} proteinase K, 60 mM EDTA, and 4 M urea) for 15 min at 37 °C. The reactions were then denatured with 4.5 M urea denaturing buffer at 95 °C for 5 min. Samples were analysed by denaturing gel electrophoresis on 10% PAGE TBE-Urea (Invitrogen) run at 45 °C. Gels were imaged using an Odyssey scanner (LI-COR Biosciences). For gel source data, see Supplementary Fig. 1.

Collateral activity detection assays were performed as previously described[9]. In brief, reactions consisted of 45 nM purified LwaCas13a, 22.5 nM crRNA, 125 nM quenched fluorescent RNA reporter (RNase Alert v2, Thermo Scientific), 2 µl mouse RNase inhibitor (New England Biolabs), 100 ng of background total

© 2017 Macmillan Publishers Limited, part of Springer Nature. All rights reserved.

human RNA (purified from HEK293FT culture), and varying amounts of input nucleic-acid target, unless otherwise indicated, in nuclease assay buffer (40 mM Tris-HCl, 60 mM NaCl, 6 mM $MgCl_2$, pH 7.3). Reactions were allowed to proceed for 1–3 h at 37 °C (unless otherwise indicated) on a fluorescent plate reader (BioTek) with fluorescent kinetics measured every 5 min.

Cloning of tiling guide screens. For tiling guide screens, spacers were designed to target mRNA transcripts at even intervals to fully cover the entire length of the transcript. Spacers (ordered from IDT) were annealed and golden-gate cloned into LwaCas13a guide expression constructs with either a $tRNA^{val}$ promoter (Gluc and Cluc screens) or U6 promoter (all endogenous screens). The guide sequences for the tiling screens are listed in Supplementary Table 7.

Mammalian cell culture and transfection for knockdown with LwaCas13a. All mammalian cell experiments were performed in the HEK293FT line (American Type Culture Collection (ATCC)) unless otherwise noted. HEK293FT cells were cultured in Dulbecco's Modified Eagle Medium with high glucose, sodium pyruvate, and GlutaMAX (Thermo Fisher Scientific) supplemented with 10% fetal bovine serum (VWR Seradigm) and 1× penicillin–streptomycin (Thermo Fisher Scientific). Cells were passaged to maintain confluency below 70%. For experiments involving A375 (ATCC), cells were cultured in RPMI Medium 1640 (Thermo Fisher Scientific) supplemented with 9% fetal bovine serum (VWR Seradigm) and 1× penicillin–streptomycin (Thermo Fisher Scientific). The HEK293FT cells were not authenticated after receiving them from ATCC and were not checked for mycoplasma contamination.

To test knockdown of endogenous genes, Lipofectamine 2000 (Thermo Fisher Scientific) transfections were performed with 150 ng of LwaCas13a plasmid and 250 ng of guide plasmid per well, unless otherwise noted. Experiments testing knockdown of reporter plasmids were supplemented with 12.5 ng reporter construct per well. Sixteen hours before transfection, cells were plated in 96-well plates at approximately 20,000 cells per well and allowed to grow to 90% confluency overnight. For each well, plasmids were combined with Opti-MEM I Reduced Serum Medium (Thermo Fisher) to a total of 25 μl, and separately 0.5 μl of Lipofectamine 2000 was combined with 24.5 μl of Opti-MEM. Plasmid and Lipofectamine solutions were then combined, incubated for 5 min, and slowly pipetted onto cells to prevent disruption.

Transformation of green rice protoplasts. For the green rice experiments, plasmids expressing each LwaCas13a and the corresponding guide RNA were mixed in equimolar ratios such that a total of 30 μg of DNA was used to transform a total of 200,000 protoplasts per transformation.

Measurement of luciferase activity. Media containing secreted luciferase was harvested 48 h after transfection, unless otherwise noted. Media were diluted 1:5 in PBS and then luciferase activity was measured using BioLux *Cypridinia* and Biolux *Gaussia* luciferase assay kits (New England Biolabs) on a Biotek Synergy 4 plate reader with an injection protocol. All replicates were performed as biological replicates.

Harvest of total RNA and quantitative PCR. For gene expression experiments in mammalian cells, cell harvesting and reverse transcription for cDNA generation was performed using a previously described modification[23] of the commercial Cells-to-Ct kit (Thermo Fisher Scientific) 48 h after transfection. Transcript expression was then quantified with qPCR using Fast Advanced Master Mix (Thermo Fisher Scientific) and TaqMan qPCR probes (Thermo Fisher Scientific, Supplementary Tables 8 and 9) with *GAPDH* control probes (Thermo Fisher Scientific). All qPCR reactions were performed in 5-μl reactions with four technical replicates in a 384-well format, and read out using a LightCycler 480 Instrument II (Roche). For multiplexed targeting reactions, readout of different targets was performed in separate wells. Expression levels were calculated by subtracting housekeeping control (*GAPDH*) cycle threshold (C_t) values from target C_t values to normalize for total input, resulting in ΔC_t levels. Relative transcript abundance was computed as $2^{-\Delta C_t}$. All replicates were performed as biological replicates.

For gene expression experiments in plant cells, total RNA was isolated after 48 h of incubation using Trizol according to the manufacturer's protocol. One nanogram of total RNA was used in a SuperScript III Plantinum SYBR Green One-Step qRT–PCR Kit (Invitrogen) according to the manufacturer's protocol. All samples were run in technical triplicate of three biological replicates in a 384-well format on a LightCycler 480 Instrument (Roche). All PCR primers were verified as being specific on the basis of melting curve analysis and were as follows: Os*EPSPS* (Os06g04280), 5′-TTGCCATGACCCTTGCCGTTGTTG-3′ and 5′-TGATGATGCAGTAGTCAGGACCTT-3′; Os*HCT* (Os11g07960), 5′-CAAGTTTGTGTACCCGAGGATTTG-3′ and 5′-AGCTAGTCCCAATAA ATATGCGCT-3′; Os*EF1a* (Os03g08020), 5′-CTGTAGTCGTTGGCTGTGGT-3′ and 5′-CAGCGTTCCCCAAGAAGAGT-3′. Primers for Os*EF1a* were previously described[24].

For analysis of RNA quality post-knockdown with LwaCas13a, total RNA was harvested by lysing cells using TRI Reagent and purifying the RNA using the Direct-zol RNA MiniPrep Plus kit (Zymo). Four nanograms of total RNA were analysed using a RNA 6000 Pico Bioanalyzer kit (Agilent).

Computational analysis of target accessibility. To first analyse target accessibility, top guides from the tiling screen were analysed to determine whether they grouped closer together than expected under the assumption that if there were regions of accessibility, multiple guides in that region would be expected to be highly active. Top guides were defined as the top 20% of performing guides for the Gluc tiling screen and top 30% of performing guides for the Cluc, *KRAS*, and *PPIB* tiling screens. A null probability distribution was generated for pairwise distances between guides by randomly simulating 10,000 guide positions and then comparing with experimentally determined top guide pairwise distances.

Accessibility was predicted using the RNApl fold algorithm in the Vienna RNA software suite[25]. The default window size of 70 nt was used and the probability of a target region being unpaired was calculated as the average of the 28 single-nucleotide unpaired probabilities across the target region. These accessibility curves were smoothed and compared with smoothed knockdown curves across each of the four transcripts, and correlations between the two factors and their significance were computed using Pearson's correlation coefficient with the SciPy Python package (pearsonr function). The probability space of these two factors was also visualized by performing two-dimensional kernel density estimation across the two variables.

RNA sequencing and analysis. For specificity analysis of LwaCas13a knockdown, RNA-seq was performed on mRNA from knockdown experiments involving both LwaCas13a and shRNA constructs. Total RNA was prepared from transfection experiments after 48 h using a Qiagen RNeasy Plus Mini kit. mRNA was then extracted using a NEBNext Poly(A) mRNA Magnetic Isolation Module and RNA-seq libraries were prepared using a NEBNext Ultra Directional RNA Library Prep Kit for Illumina. RNA-seq libraries were sequenced on an Illumina NextSeq instrument with at least 10 million reads per library.

An index was generated using the RefSeq GRCh38 assembly and reads were aligned and quantified using Bowtie and RSEM version 1.2.31 with default parameters[26]. Transcripts per million (TPM) values were used for expression counts and were transformed to log-space by taking the $\log_2(\text{TPM}+1)$.

To find differentially expressed genes, Student's *t*-test was performed on the three targeting replicates versus the three non-targeting replicates. The statistical analysis was only performed on genes that had a $\log_2(\text{TPM}+1)$ value greater than 2.5 in at least two of the six replicates. Only genes that had a differential expression greater than 2 or less than 0.75 and a false discovery rate <0.10 were reported to be significantly differentially expressed.

Cross-correlations between replicates and averages of replicates were performed using Kendall's tau coefficient. The variation of shRNA versus LwaCas13a libraries was analysed by considering the distribution of standard deviations for gene expression across the six replicates (three targeting and three non-targeting replicates) and represented as violin plots.

Cell viability assay. Mammalian cells were transfected with luciferase reporter target, guide plasmid, and either LwaCas13a or drug-selectable LwaCas13a. Twenty-four hours after transfection, cells were split 1:5 into fresh media and drug-selectable LwaCas13a samples were supplemented with 10 μg ml^{-1} Blasticidin S (Thermo Fisher Scientific). After 48 h of additional growth, cells were assayed for luciferase knockdown, maintenance of LwaCas13a expression via GFP fluorescence measurement on a multimode plate reader (Biotek Neo2), and cell growth by CellTiter-Glo Luminescent Cell Viability Assay (Promega).

Quantifying dLwaCas13a binding with RNA immunoprecipitation. For RNA immunoprecipitation experiments, HEK293FT cells were plated in six-well plates and transfected with 1.3 μg of dLwaCas13a expression plasmid and 1.7 μg of guide plasmid, with an additional 150 ng of reporter plasmid for conditions involving reporter targeting. Forty-eight hours after transfection, cells were washed twice with ice-cold PBS (Sigma) and fixed with 0.2% paraformaldehyde (Electron Microscopy Sciences) in PBS for 15 min at room temperature. After fixation, the paraformaldehyde was removed, 125 mM glycine in PBS was added to quench crosslinking, and the cells were incubated for 10 min. Cells were washed twice with ice-cold PBS, harvested by scraping, and the cell suspension was centrifuged at 800*g* for 4 min to pellet the cells. The supernatant was removed and the pellet was washed with PBS before lysis. Cells were lysed with 200 μl of 1× RIPA Buffer (Cell Signaling) supplemented with cOmplete ULTRA Tablets, EDTA-free (Sigma) and ribonuclease inhibitor (Sigma R1158). Cells were allowed to lyse on ice for 10 min and then sonicated for 2 min with a 30 s on/30 s off cycle at low intensity on a Bioruptor sonicator (Diagenode). Insoluble material was pelleted by centrifugation at 16,000*g* for 10 min at 4 °C, and the supernatant containing cleared lysate was used for pulldown with magnetic beads.

To conjugate antibodies to magnetic beads, 100 μl per sample of Dynabeads Protein A for Immunoprecipitation (Thermo Fisher Scientific) were pelleted by application of a magnet, and the supernatant was removed. Beads were resuspended

© 2017 Macmillan Publishers Limited, part of Springer Nature. All rights reserved.

in 200 μl of wash buffer (PBS supplemented with 0.02% Tween 20 (Sigma)) and 5 μg of rabbit anti-Mouse IgG (Sigma M7023) was added. The sample was incubated for 10 min at room temperature on a rotator to allow antibody to conjugate to the beads. After incubation, beads were pelleted using a magnet, supernatant was removed, and beads were washed twice with wash buffer. The pellet was resuspended in 100 μl wash buffer and split into two 50 μl volumes for conjugation of anti-HA antibody (Thermo Fisher Scientific 26183) or IgG antibody control (Sigma I5381). For each antibody, 2.5 μg of antibody was added with 200 μl wash buffer and incubated for 10 min at room temperature on a rotator. After incubation, beads were pelleted using a magnet and washed twice with wash buffer, and resuspended in 200 μl 1× RIPA with ribonuclease inhibitor (Sigma R1158) and protease inhibitor cocktail (Sigma P8340). One hundred microlitres of sample lysate were added to beads and rotated overnight at 4 °C.

After incubation with sample lysate, beads were pelleted, washed three times with 1× RIPA, 0.02% Tween 20, and then washed with DNase buffer (350 mM Tris-HCl (pH 6.5); 50 mM $MgCl_2$; 5 mM DTT). Beads were resuspended in DNase buffer and TURBO DNase (Life Technologies) was added to a final concentration of 0.08 units per microlitre. DNase was incubated for 30 min at 37 °C on a rotator. Proteins were then digested by addition of Proteinase K (New England Biosciences) to a final concentration of 0.1 units per microlitre and incubated at 37 °C with rotation for an additional 30 min. For denaturation and purification, urea (Sigma) was added to a final concentration of 2.5 M, samples were incubated for 30 min, and RNA was purified using a Direct-Zol RNA miniprep (Zymo Research). Purified RNA was reverse transcribed to cDNA using the qScript Flex cDNA (Quantabio) and pulldown was quantified with qPCR using Fast Advanced Master Mix and TaqMan qPCR probes (Supplementary Tables 8 and 9). All qPCR reactions were performed in 5-μl reactions with 4 technical replicates in 384-well format, and read out using a LightCycler 480 Instrument II. Enrichment was quantified for samples compared with their matched IgG antibody controls.

Translocation measurement of LwaCas13a and LwaCas13a-NF. HEK293FT cells were plated in 24-well tissue culture plates on poly-D-lysine coverslips (Corning) and transfected with 150 ng dLwaCas13a–NF vector and 300 ng guides for imaging *ACTB*. For translocation experiments, cells were fixed with 4% PFA, permeabilized with 0.2% Triton X-100 after 48 h, and mounted using anti-fade mounting medium with DAPI (Vectashield). Confocal microscopy was performed with a Nikon Eclipse Ti1 with Andor Yokagawa Spinning disk Revolution WD system.

Nuclear export of dLwaCas13a-NF with guides targeting *ACTB* mRNA was analysed by measuring the average cytoplasmic and nuclear msfGFP fluorescence and comparing the ratio across many cells between targeting and non-targeting conditions.

FISH of *ACTB* transcript. HEK293FT cells were plated in 24-well tissue culture plates on poly-D-lysine coverslips (Corning) and transfected with 75 ng dLwaCas13a–NF vector and 250 ng guides for imaging *ACTB*. After 48 h, cells were fixed with 4% PFA for 45 min. A QuantiGene viewRNA ISH Cell assay kit (Affymetrix) was used for performing FISH on the cell samples according to the manufacturer's protocol. After finishing the FISH procedure, coverslips were mounted using anti-fade mounting medium (Vectashield). Confocal microscopy was performed using a Nikon Eclipse Ti1 with Andor Yokagawa Spinning disk Revolution WD system.

Tracking of LwaCas13a to stress granules. HEK293FT cells were plated in 24-well tissue culture plates on poly-D-lysine coverslips (Corning) and transfected with 75 ng dLwaCas13a-NF vector and 250 ng guides for imaging *ACTB*. For stress granule experiments, 200 μM sodium arsenite was applied for 1 h before fixing and permeabilizing the cells. For immunofluorescence of G3BP1, cells were blocked with 20% goat serum, and incubated overnight at room temperature with anti-G3BP1 primary antibody (Abnova H00010146-B01P). Cells were then incubated for 1 h with secondary antibody labelled with Alexa Fluor 594 and mounted using anti-fade mounting medium with DAPI (Vectashield). Confocal microscopy was performed using a Nikon Eclipse Ti1 with Andor Yokagawa Spinning disk Revolution WD system.

Stress granule co-localization with dLwaCas13a–NF was calculated using the average msfGFP and G3BP1 signal per cell using Pearson's correlation coefficient. The co-localization analyses were performed in the image analysis software FIJI[27] using the Coloc 2 plugin.

For live imaging experiments, HEK293FT cells were plated in 96-well tissue culture plates and transfected with 150 ng dLwaCas13a–NF vector, 300 ng guides for imaging *ACTB*, and 5 ng of G3BP1–RFP reporter. After 48 h, the cells were subjected to 0 μM or 400 μM sodium arsenite and imaged every 15 min for 2 h on an Opera Phenix High Content Screening System (PerkinElmer) using the spinning disk confocal setting with a 20× water objective. Cells were maintained at 37 °C in a humidified chamber with 50% CO_2. Live-cell dLwaCas13a–NF co-localization with G3BP1–RFP in stress granules was measured using Opera Phenix Harmony software (PerkinElmer).

Data availability. LwaCas13a (C2c2) expression plasmids are available from Addgene under UBMTA. Patent applications have been filed relating to work in this manuscript. Support forums and computational tools including relevant code for data analysis are available via the Zhang laboratory website (http://www.genome-engineering.org) and Github (https://github.com/fengzhanglab). High-throughput sequencing data related to this study are available at BioProject under accession number PRJNA383832. Raw data represented in main figures in this study are included in this published article and its Supplementary Information. Additional datasets are available from the corresponding author on reasonable request.

20. Tafer, H. *et al.* The impact of target site accessibility on the design of effective siRNAs. *Nat. Biotechnol.* **26,** 578–583 (2008).
21. Mann, D. G. *et al.* Gateway-compatible vectors for high-throughput gene functional analysis in switchgrass (*Panicum virgatum* L.) and other monocot species. *Plant Biotechnol. J.* **10,** 226–236 (2012).
22. Zhang, Y. *et al.* A highly efficient rice green tissue protoplast system for transient gene expression and studying light/chloroplast-related processes. *Plant Methods* **7,** 30 (2011).
23. Joung, J. *et al.* Genome-scale CRISPR–Cas9 knockout and transcriptional activation screening. *Nat. Protocols* **12,** 828–863 (2017).
24. Jain, M., Nijhawan, A., Tyagi, A. K. & Khurana, J. P. Validation of housekeeping genes as internal control for studying gene expression in rice by quantitative real-time PCR. *Biochem. Biophys. Res. Commun.* **345,** 646–651 (2006).
25. Bernhart, S. H., Hofacker, I. L. & Stadler, P. F. Local RNA base pairing probabilities in large sequences. *Bioinformatics* **22,** 614–615 (2006).
26. Li, B. & Dewey, C. N. RSEM: accurate transcript quantification from RNA-Seq data with or without a reference genome. *BMC Bioinformatics* **12,** 323 (2011).
27. Schindelin, J. *et al.* Fiji: an open-source platform for biological-image analysis. *Nat. Methods* **9,** 676–682 (2012).

© 2017 Macmillan Publishers Limited, part of Springer Nature. All rights reserved.

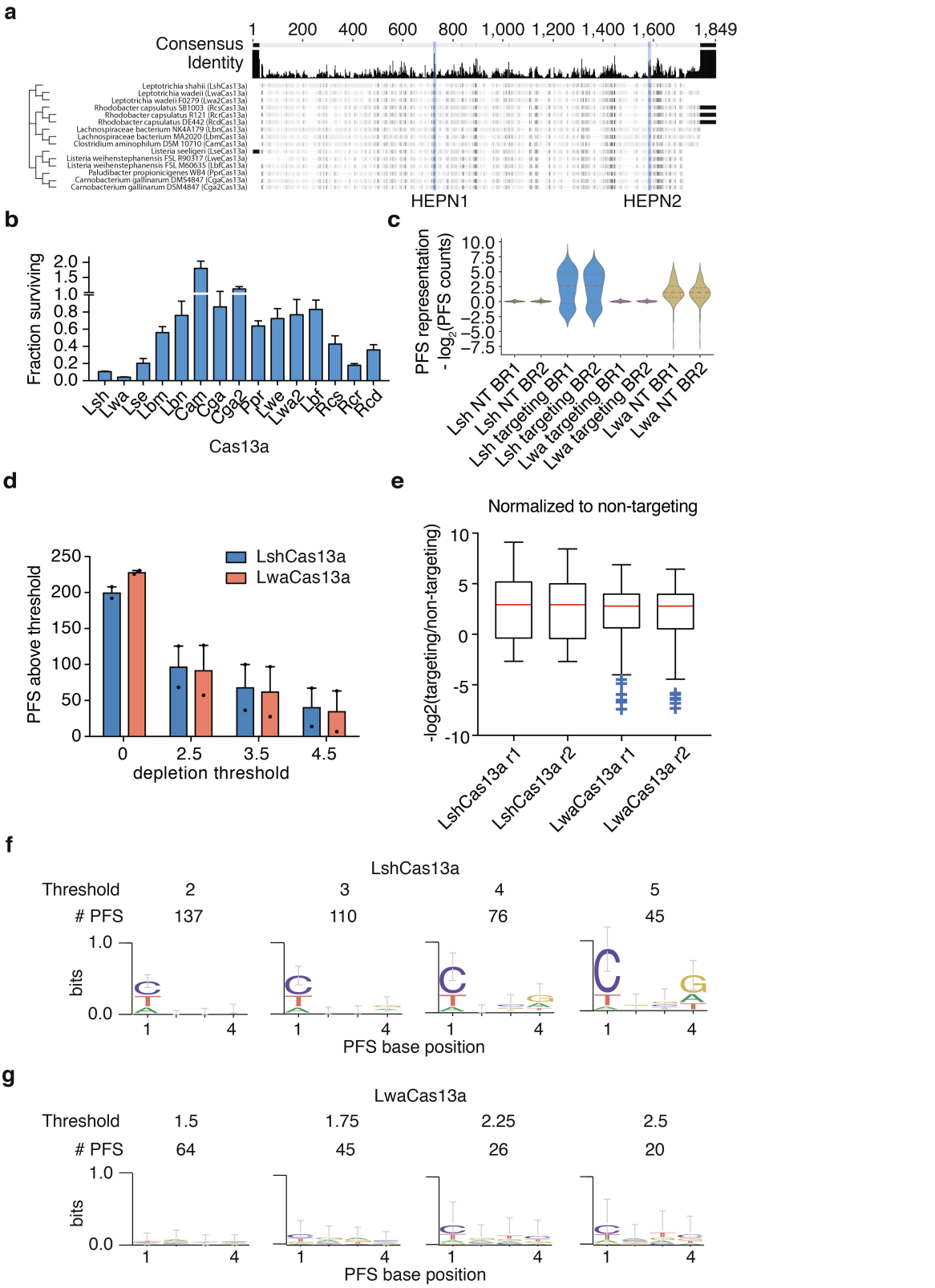

Extended Data Figure 1 | Evaluation of LwaCas13a PFS preferences and comparisons with LshCas13a. a, Sequence comparison tree of the 15 Cas13a orthologues evaluated in this study. **b**, Ratios of *in vivo* activity from Fig. 1b. **c**, Distributions of PFS enrichment for LshCas13a and LwaCas13a in targeting and non-targeting samples. The 25th and 75th percentiles are shown as grey dotted lines and the median is shown as a red dotted line. The minimum and maximum are marked by the ends of the distribution. Each distribution represents 976 PFS sequences ($n = 976$). **d**, Number of LshCas13a and LwaCas13a PFS sequences above depletion threshold for varying depletion thresholds. Values are mean ± s.e.m. with $n = 2$. **e**, Distributions of PFS enrichment for LshCas13a and LwaCas13a in targeting samples, normalized to non-targeting samples. The 25th and 75th percentiles are marked by the ends of the box and the median is shown as a red line within the box. Whiskers denote 1.5 times the interquartile range; blue '+' denote outliers that are beyond 1.5 times the interquartile range. Each distribution represents 976 PFS sequences ($n = 976$). **f**, Sequence logos and counts for remaining PFS sequences after LshCas13a cleavage at varying enrichment cutoff thresholds. **g**, Sequence logos and counts for remaining PFS sequences after LwaCas13a cleavage at varying enrichment cutoff thresholds.

© 2017 Macmillan Publishers Limited, part of Springer Nature. All rights reserved.

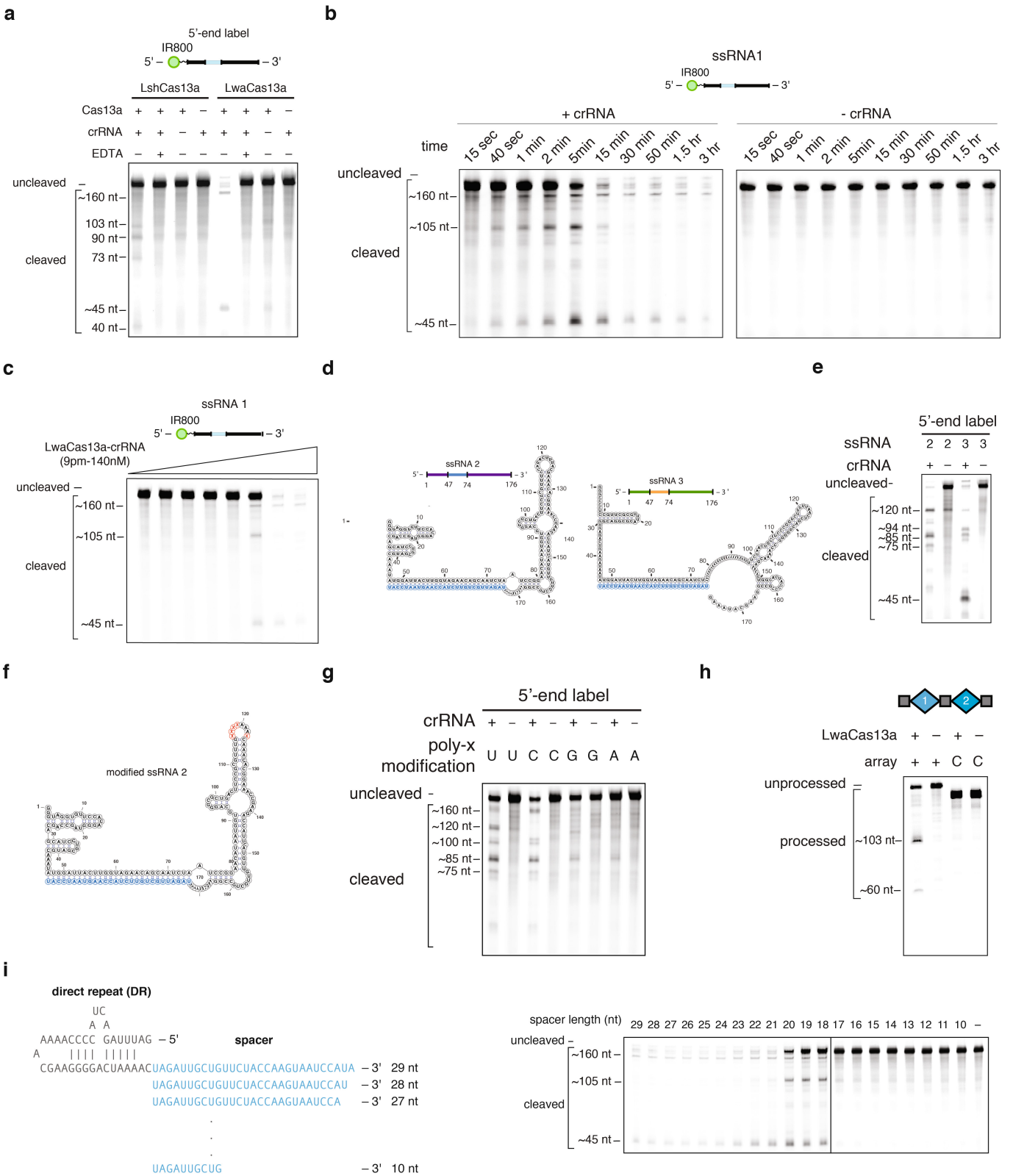

Extended Data Figure 2 | Biochemical characterization of LwaCas13a RNA cleavage activity. a, Gel electrophoresis comparison of LwaCas13a and LshCas13a RNase activity on ssRNA 1. **b**, Gel electrophoresis of ssRNA1 after incubation with LwaCas13a with or without crRNA 1 for varying amounts of times. **c**, Gel electrophoresis of ssRNA 1 after incubation with varying amounts of LwaCas13a–crRNA complex. **d**, Sequence and structure of ssRNA 4 and ssRNA 5. crRNA spacer sequence is highlighted in blue. **e**, Gel electrophoresis of ssRNA 4 and ssRNA 5 after incubation with LwaCas13a and crRNA 1. **f**, Sequence and structure of ssRNA 4 with sites of poly-x modifications highlighted in red. crRNA spacer sequence is highlighted in blue. **g**, Gel electrophoresis of ssRNA 4 with each of four possible poly-x modifications incubated with LwaCas13a and crRNA 1. **h**, Gel electrophoresis of pre-crRNA from the *L. wadei* CRISPR–Cas locus showing LwaCas13a processing activity. **i**, Cleavage efficiency of ssRNA 1 for crRNA spacer truncations after incubation with LwaCas13a. For gel source data, see Supplementary Fig. 1.

© 2017 Macmillan Publishers Limited, part of Springer Nature. All rights reserved.

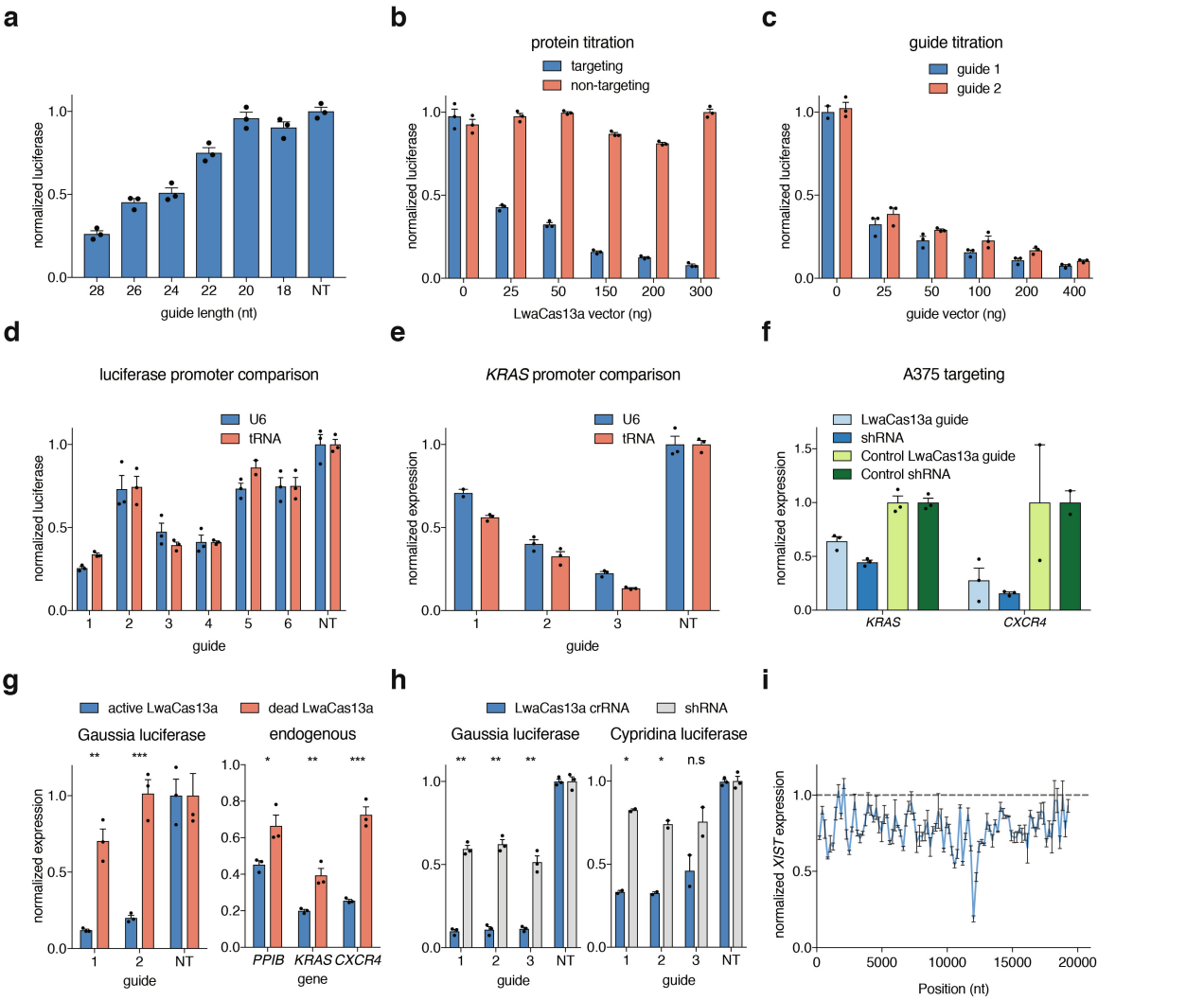

Extended Data Figure 3 | Engineering and optimization of LwaCas13a for mammalian knockdown. a, Knockdown of Gluc transcript by LwaCas13a and Gluc guide 1 spacers of varying length. **b**, Knockdown of Gluc transcript with Gluc guide 1 and varying amounts of transfected LwaCas13a plasmid. **c**, Knockdown of Gluc transcript by LwaCas13a and varying amounts of transfected Gluc guide 1 and 2 plasmid ($n = 2$ or 3). **d**, Knockdown of Gluc transcript using guides expressed from either U6 or $tRNA^{Val}$ promoters ($n = 2$ or 3). **e**, Knockdown of *KRAS* transcript using guides expressed from either U6 or $tRNA^{Val}$ promoters ($n = 2$ or 3). **f**, Knockdown of *KRAS* and *CXCR4* transcripts by LwaCas13a using guides transfected in A375 cells with position-matched shRNA comparisons ($n = 2$ or 3). **g**, Knockdown of Gluc transcript and endogenous transcripts *PPIB*, *KRAS*, and *CXCR4* with active and catalytically inactive LwaCas13a. **h**, Validation of the top three guides from the arrayed knockdown Gluc and Cluc screens with shRNA comparisons ($n = 2$ or 3). **i**, Arrayed knockdown screen of 93 guides evenly tiled across the *XIST* transcript. All values are mean ± s.e.m. with $n = 3$, unless otherwise noted (n represents the number of transfection replicates). $^{***}P < 0.001$; $^{**}P < 0.01$; $^{*}P < 0.05$. n.s, not significant. A two-tailed Student's t-test was used for comparisons.

© 2017 Macmillan Publishers Limited, part of Springer Nature. All rights reserved.

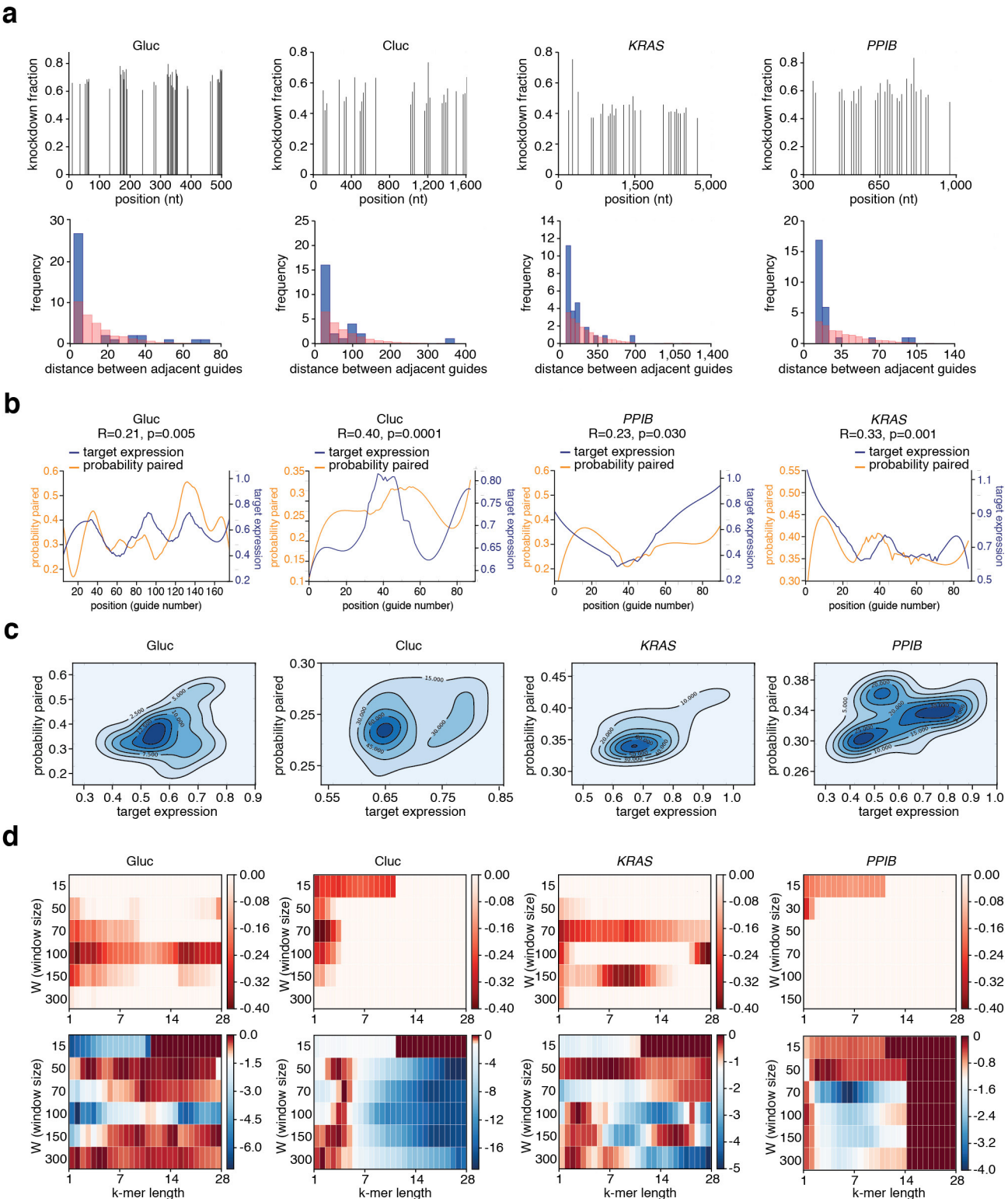

Extended Data Figure 4 | LwaCas13a targeting efficiency is influenced by accessibility along the transcript. a, Top row: top knockdown guides are plotted by position along target transcript. Top knockdown guides are defined as the top 20% of guides for Gluc and the top 30% of guides for Cluc, *KRAS*, and *PPIB*. Bottom row: histograms for the pairwise distance between adjacent top guides for each transcript (blue) compared with a random null distribution (red). A shift of the blue curve (actual measured distances) to the left of the red curve (null distribution of distances) indicates that guides are closer together than expected by chance. **b**, Gluc, Cluc, *PPIB*, and *KRAS* knockdown partly correlates with target accessibility as measured by predicted folding of the transcript. The correlation was computed using a Pearson's correlation coefficient and two-tailed Student's *t*-test. **c**, Kernel density estimation plots depicting the correlation between target accessibility (probability of a region being base-paired) and target expression after knockdown by LwaCas13a. **d**, Top row: correlations between target expression and target accessibility (probability of a region being base-paired) measured at different window sizes (W) and for different *k*-mer lengths. Bottom row: *P* values for the correlations between target expression and target accessibility (probability of a region being base-paired) measured at different window sizes (W) and for different *k*-mer lengths. The colour scale is designed such that *P* values >0.05 are shades of red and *P* values <0.05 are shades of blue.

© 2017 Macmillan Publishers Limited, part of Springer Nature. All rights reserved.

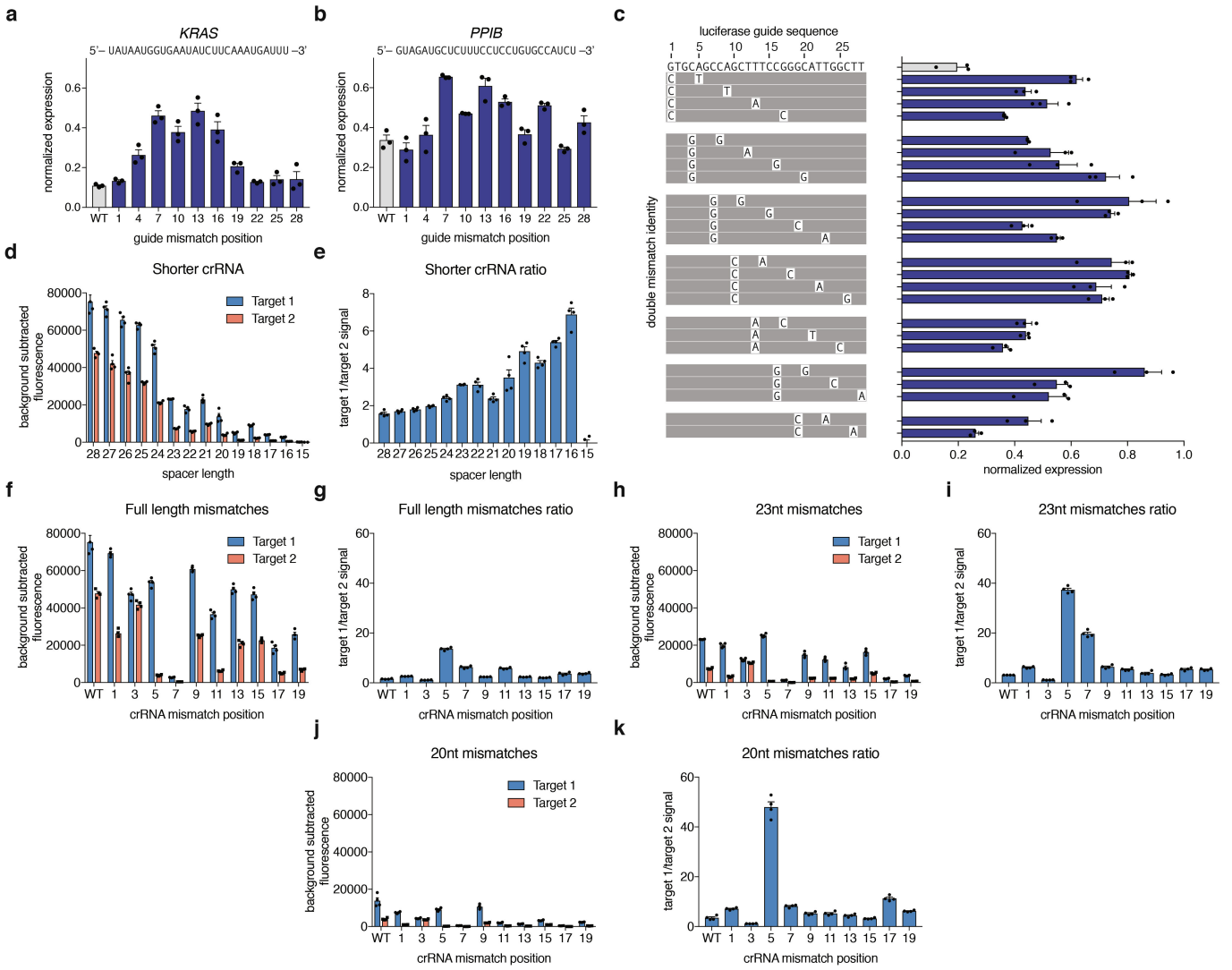

Extended Data Figure 5 | Detailed evaluation of LwaCas13a sensitivity to mismatches in the guide–target duplex at varying spacer lengths. **a**, Knockdown of *KRAS* evaluated with guides containing single mismatches at varying positions across the spacer sequence ($n = 2$ or 3). **b**, Knockdown of *PPIB* evaluated with guides containing single mismatches at varying positions across the spacer sequence ($n = 2$ or 3). **c**, Knockdown of Gluc evaluated with guides containing non-consecutive double mismatches at varying positions across the spacer sequence. The wild-type sequence is shown at the top with mismatch identities shown below. **d**, Collateral cleavage activity on ssRNA 1 and 2 for varying spacer lengths. **e**, Specificity ratios of guide tested in **d**. Specificity ratios are calculated as the ratio of the on-target RNA (ssRNA 1) collateral cleavage to the off-target RNA (ssRNA 2) collateral cleavage. **f**, Collateral cleavage activity on ssRNA 1 and 2 for 28-nt spacer crRNA with synthetic mismatches tiled along the spacer. **g**, Specificity ratios, as defined in **e**, of crRNA tested in **f**. **h**, Collateral cleavage activity on ssRNA 1 and 2 for 23-nt spacer crRNA with synthetic mismatches tiled along the spacer. **i**, Specificity ratios, as defined in **e**, of crRNA tested in **h**. **j**, Collateral cleavage activity on ssRNA 1 and 2 for 20-nt spacer crRNA with synthetic mismatches tiled along the spacer. **k**, Specificity ratios, as defined in **e**, of crRNA tested in **j**. For **a**–**c**, all values are mean ± s.e.m. with $n = 3$, unless otherwise noted (n represents the number of transfection replicates). For **d**–**k**, all values are mean ± s.e.m. with $n = 4$ (n represents the number of technical replicates).

© 2017 Macmillan Publishers Limited, part of Springer Nature. All rights reserved.

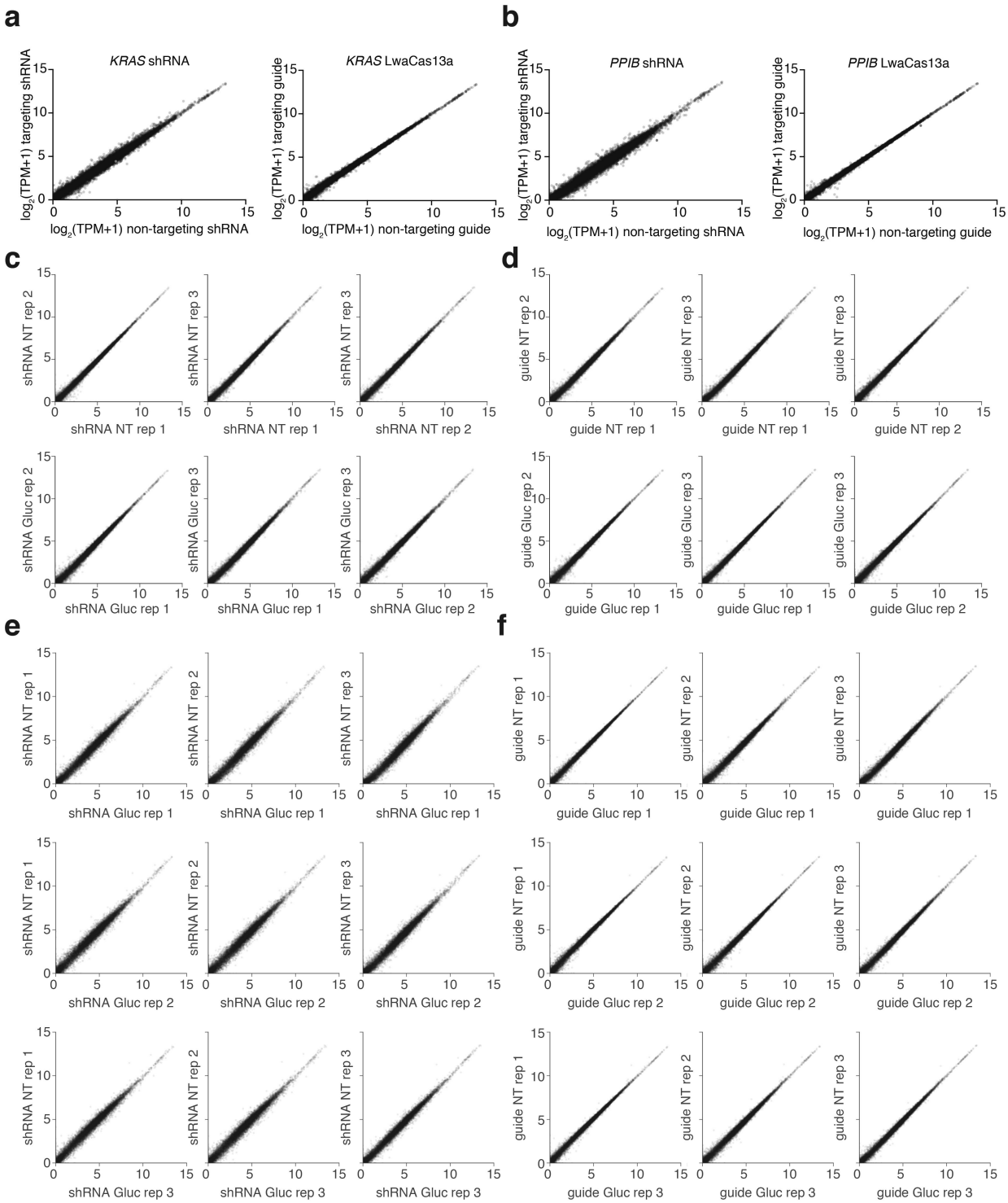

Extended Data Figure 6 | LwaCas13a is more specific than shRNA knockdown for endogenous targets. a, Left: expression levels in $\log_2$(transcripts per million (TPM) + 1) values of all genes detected in RNA-seq libraries of non-targeting shRNA-transfected control (*x* axis) compared with *KRAS*-targeting shRNA (*y* axis). Shown is the mean of three biological replicates. The *KRAS* transcript data point is coloured in red. Right: expression levels in $\log_2$(transcripts per million (TPM) + 1) values of all genes detected in RNA-seq libraries of non-targeting LwaCas13a-guide-transfected control (*x* axis) compared with *KRAS*-targeting LwaCas13a-guide (*y* axis). Shown is the mean of three biological replicates. The *KRAS* transcript data point is coloured in red. **b**, Left: expression levels in $\log_2$(transcripts per million (TPM) + 1) values of all genes detected in RNA-seq libraries of non-targeting shRNA-transfected control (*x* axis) compared with *PPIB*-targeting shRNA (*y* axis). Shown is the mean of three biological replicates. The *PPIB* transcript data point is coloured in red. Right: expression levels in $\log_2$(transcripts per million (TPM) + 1) values of all genes detected in RNA-seq libraries of non-targeting LwaCas13a-guide-transfected control (*x* axis) compared with *PPIB*-targeting LwaCas13a-guide (*y* axis). Shown is the mean of three biological replicates. The *PPIB* transcript data point is coloured in red. **c**, Comparisons of individual replicates of non-targeting shRNA conditions (top row) and Gluc-targeting shRNA conditions (bottom row). **d**, Comparisons of individual replicates of non-targeting guide conditions (top row) and Gluc-targeting guide conditions (bottom row). **e**, Pairwise comparisons of individual replicates of non-targeting shRNA conditions against the Gluc-targeting shRNA conditions. **f**, Pairwise comparisons of individual replicates of non-targeting guide conditions against the Gluc-targeting guide conditions.

© 2017 Macmillan Publishers Limited, part of Springer Nature. All rights reserved.

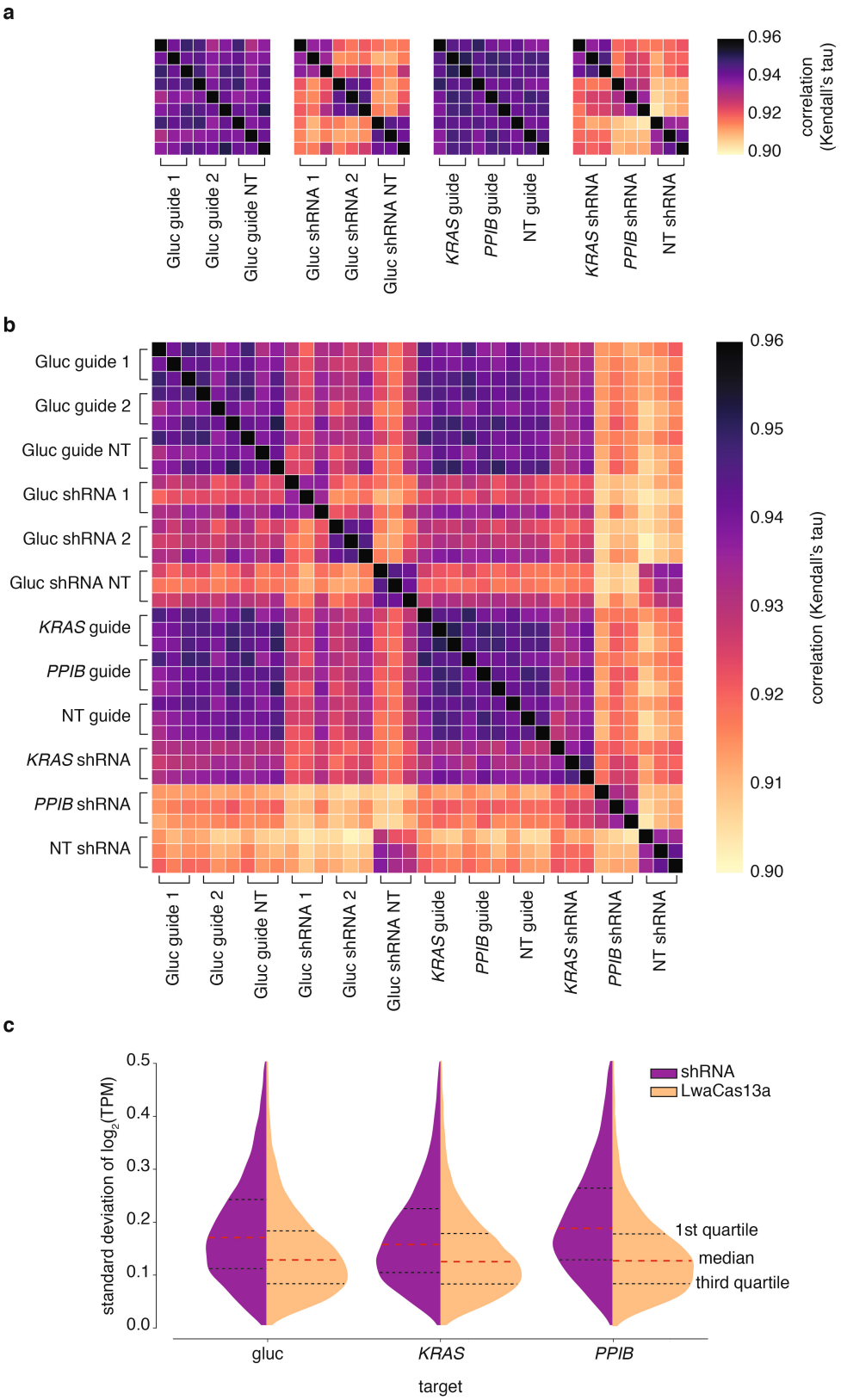

Extended Data Figure 7 | Detailed analysis of LwaCas13a and RNAi knockdown variability (standard deviation) across all samples. **a**, Heatmap of correlations (Kendall's tau) for $\log_2$(transcripts per million (TPM + 1)) values of all genes detected in RNA-seq libraries between targeting and non-targeting replicates for shRNA or guide targeting either luciferase reporters or endogenous genes. **b**, Heatmap of correlations (Kendall's tau) for $\log_2$(transcripts per million (TPM + 1)) values of all genes detected in RNA-seq libraries between all replicates and perturbations. **c**, Distributions of standard deviations for $\log_2$(transcripts per million (TPM + 1)) values of all genes detected in RNA-seq libraries among targeting and non-targeting replicates for each gene targeted by either shRNA or guide.

© 2017 Macmillan Publishers Limited, part of Springer Nature. All rights reserved.

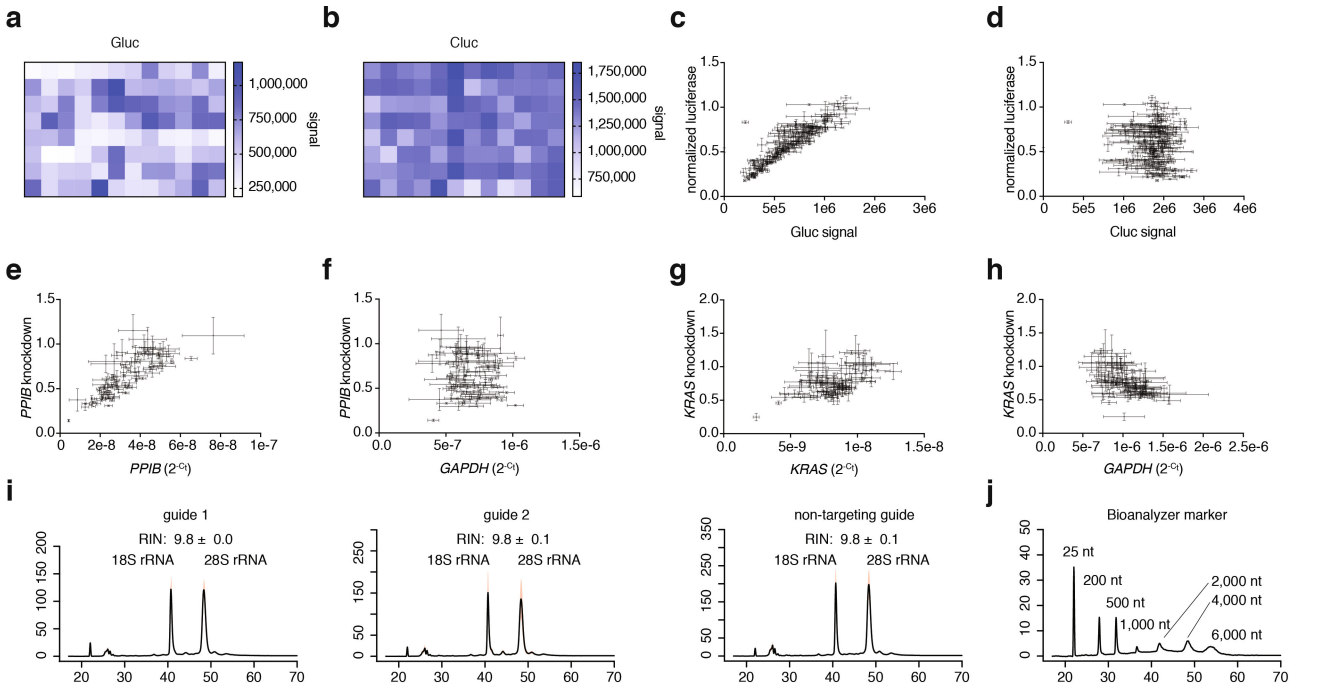

Extended Data Figure 8 | LwaCas13a knockdown is specific to the targeted transcript with no activity on a measured off-target transcript. a, Heatmap of absolute Gluc signal for first 96 spacers tiling Gluc. **b**, Heatmap of absolute Cluc signal for first 96 spacers tiling Gluc. **c**, Relationship between absolute Gluc signal and normalized luciferase for Gluc tiling guides. **d**, Relationship between absolute Cluc signal and normalized luciferase for Gluc tiling guides. **e**, Relationship between *PPIB* 2^{-C_t} levels and *PPIB* knockdown for *PPIB* tiling guides. **f**, Relationship between *GAPDH* 2^{-C_t} levels and *PPIB* knockdown for *PPIB* tiling guides. **g**, Relationship between *KRAS* 2^{-C_t} levels and *KRAS* knockdown for *KRAS* guides. **h**, Relationship between *GAPDH* 2^{-C_t} levels and *KRAS* knockdown for *KRAS* guides. **i**, Bioanalyzer traces of total RNA isolated from cells transfected with Gluc-targeting guides 1 and 2 or non-targeting guide from the experiment with active LwaCas13a in Extended Data Fig. 3g. The RNA integrity number (RIN) is shown and 18S rRNA and 28S rRNA peaks are labelled above. A Student's *t*-test showed no significant difference for the RIN between either of the targeting conditions and the non-targeting condition. The curves are shown as a mean of three replicates and the shaded areas in light red around the curves show the s.e.m. **j**, The Bioanalyzer trace for the RNA ladder with peak sizes labelled above.

© 2017 Macmillan Publishers Limited, part of Springer Nature. All rights reserved.

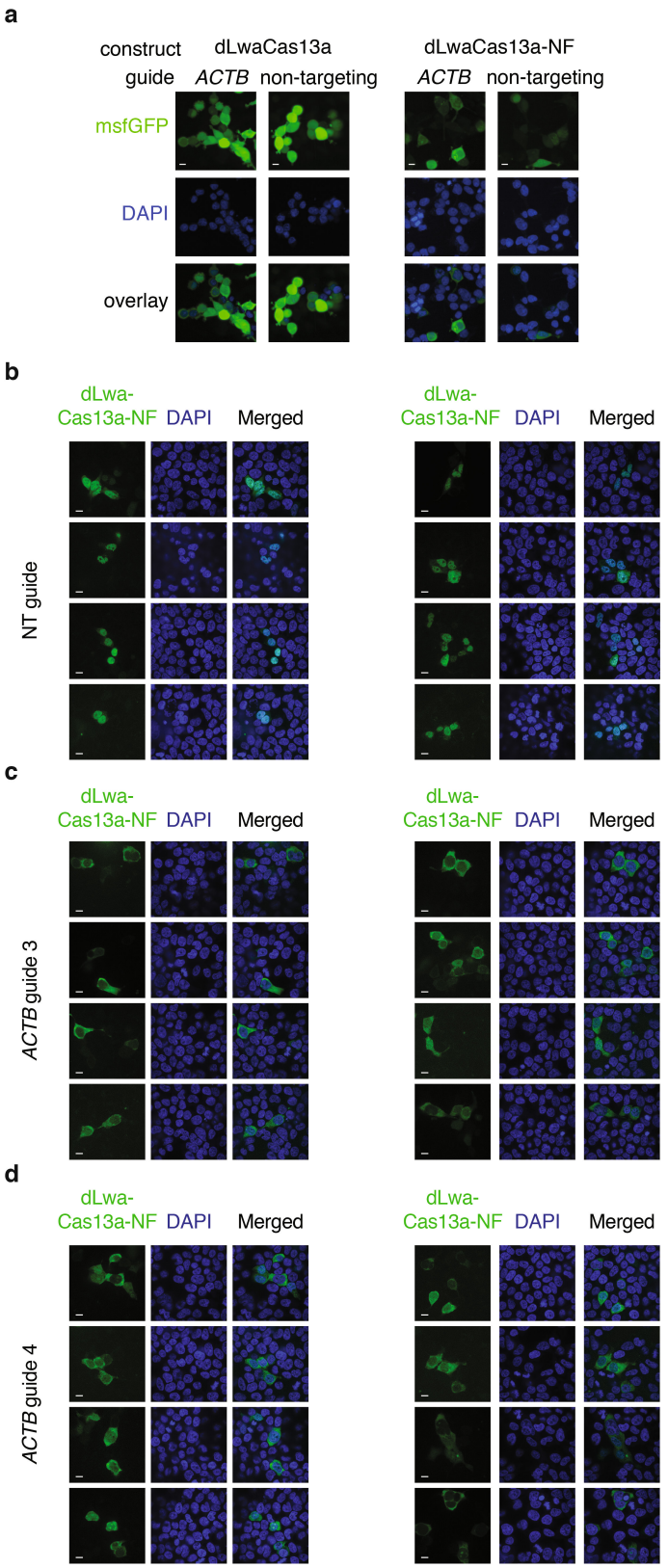

Extended Data Figure 9 | dLwaCas13a–NF can be used for *ACTB* imaging. a, Comparison between localization of dLwaCas13–GFP and dLwaCas13a–GFP–KRAB (dLwaCas13a–NF) constructs for imaging *ACTB*. Scale bars, 10 μm. **b**, Additional fields of view of dLwaCas13a–NF delivered with a non-targeting guide. Scale bars, 10 μm. **c**, Additional fields of view of dLwaCas13a–NF delivered with *ACTB* guide 3. Scale bars, 10 μm. **d**, Additional fields of view of dLwaCas13a–NF delivered with *ACTB* guide 4. Scale bars, 10 μm.

© 2017 Macmillan Publishers Limited, part of Springer Nature. All rights reserved.

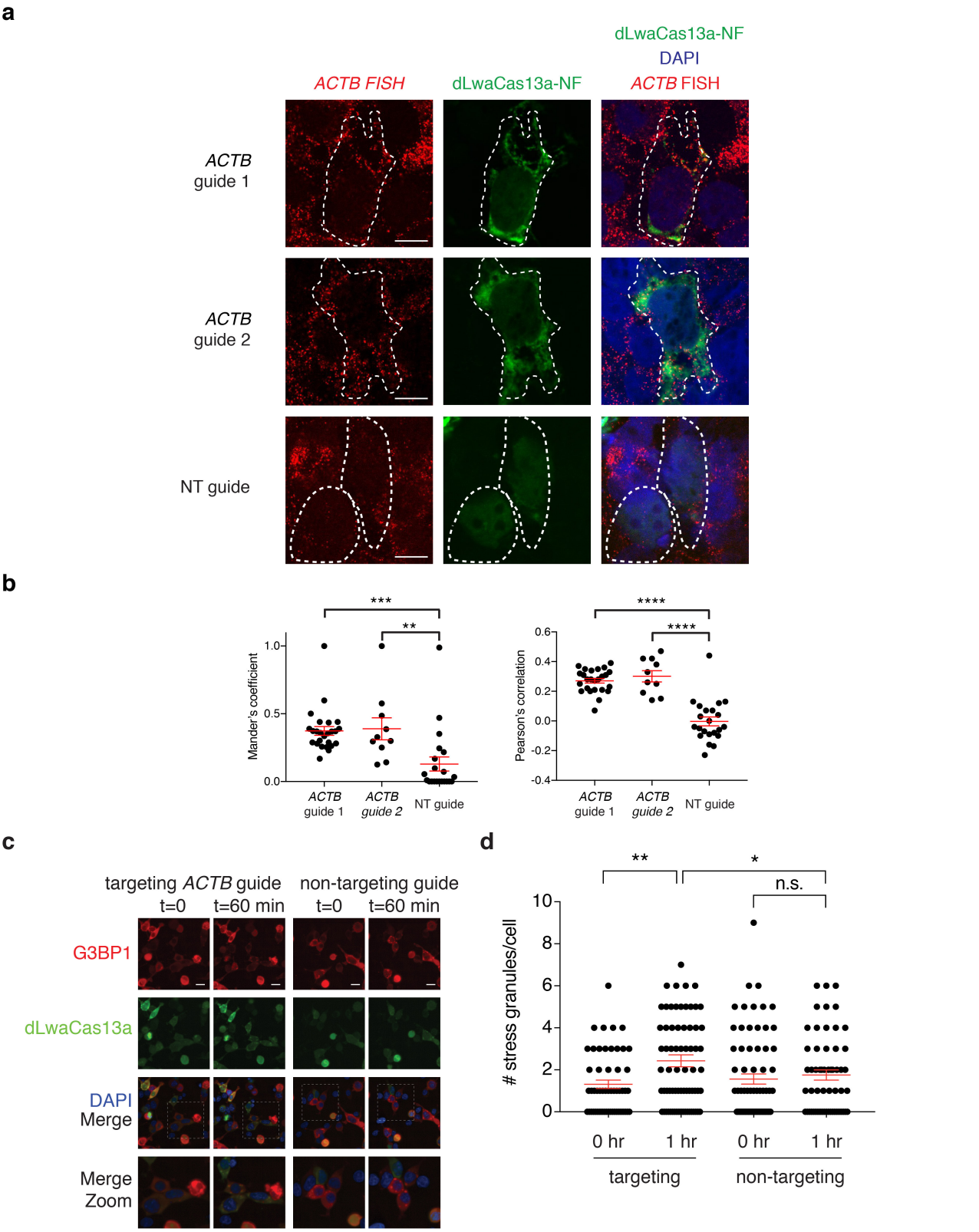

Extended Data Figure 10 | dLwaCas13a–NF can image stress granule formation in living cells. a, Representative images from RNA FISH of the *ACTB* transcript in dLwaCas13a–NF-expressing cells with corresponding *ACTB*-targeting and non-targeting guides. Cell outline is shown with a dashed line. Scale bars, 10 μm. **b**, Overall signal overlap between *ACTB* RNA FISH signal and dLwaCas13a–NF quantified by the Mander's overlap coefficient (left) and Pearson's correlation (right). Correlations and signal overlap were calculated pixel-by-pixel on a per cell basis; $n = 10–25$ cells per condition. $^{****}P < 0.0001$; $^{***}P < 0.001$; $^{**}P < 0.01$. A two-tailed Student's *t*-test was used for comparisons. **c**, Representative images from live-cell analysis of stress granule formation in response to 400 μM sodium arsenite treatment. Scale bars, 20 μm. **d**, Quantification of stress granule formation in response to sodium arsenite treatment. Quantification is based on overlapping dLwaCas13a–NF and G3BP1 puncta; $n = 54–72$ cells per condition. All values are mean ± s.e.m. $^{****}P < 0.0001$; $^{***}P < 0.001$; $^{**}P < 0.01$; $^{*}P < 0.05$. n.s., not significant. A two-tailed Student's *t*-test was used for comparisons.

© 2017 Macmillan Publishers Limited, part of Springer Nature. All rights reserved.

nature research

Corresponding author(s): Feng Zhang

☐ Initial submission ☒ Revised version ☐ Final submission

Life Sciences Reporting Summary

Nature Research wishes to improve the reproducibility of the work that we publish. This form is intended for publication with all accepted life science papers and provides structure for consistency and transparency in reporting. Every life science submission will use this form; some list items might not apply to an individual manuscript, but all fields must be completed for clarity.

For further information on the points included in this form, see Reporting Life Sciences Research. For further information on Nature Research policies, including our data availability policy, see Authors & Referees and the Editorial Policy Checklist.

Experimental design

1. Sample size

Describe how sample size was determined.

Sample sizes were not predetermined. At least 3 biological replicates were used for experiments, as is standard practice.

2. Data exclusions

Describe any data exclusions.

For tiling and multiplexing experiments, biological replicates that were drastic outliers due to experimental variability were excluded.

3. Replication

Describe whether the experimental findings were reliably reproduced.

All attempts at replications were successful.

4. Randomization

Describe how samples/organisms/participants were allocated into experimental groups.

This is not relevant to biochemical/cell biology studies and samples were not randomized.

5. Blinding

Describe whether the investigators were blinded to group allocation during data collection and/or analysis.

This is not relevant to biochemical/cell biology studies and samples were not blinded.

Note: all studies involving animals and/or human research participants must disclose whether blinding and randomization were used.

6. Statistical parameters

For all figures and tables that use statistical methods, confirm that the following items are present in relevant figure legends (or in the Methods section if additional space is needed).

n/a	Confirmed	
☐	☒	The exact sample size (*n*) for each experimental group/condition, given as a discrete number and unit of measurement (animals, litters, cultures, etc.)
☐	☒	A description of how samples were collected, noting whether measurements were taken from distinct samples or whether the same sample was measured repeatedly
☒	☐	A statement indicating how many times each experiment was replicated
☐	☒	The statistical test(s) used and whether they are one- or two-sided (note: only common tests should be described solely by name; more complex techniques should be described in the Methods section)
☐	☒	A description of any assumptions or corrections, such as an adjustment for multiple comparisons
☐	☒	The test results (e.g. *P* values) given as exact values whenever possible and with confidence intervals noted
☐	☒	A clear description of statistics including central tendency (e.g. median, mean) and variation (e.g. standard deviation, interquartile range)
☐	☒	Clearly defined error bars

See the web collection on statistics for biologists for further resources and guidance.

Software

Policy information about availability of computer code

7. Software

Describe the software used to analyze the data in this study.	Data was analyzed in Graphpad Prism 7, imaging data was analyzed in Fiji 2.0, and scripts were written in Python 2.7.

For manuscripts utilizing custom algorithms or software that are central to the paper but not yet described in the published literature, software must be made available to editors and reviewers upon request. We strongly encourage code deposition in a community repository (e.g. GitHub). *Nature Methods* guidance for providing algorithms and software for publication provides further information on this topic.

Materials and reagents

Policy information about availability of materials

8. Materials availability

Indicate whether there are restrictions on availability of unique materials or if these materials are only available for distribution by a for-profit company.	No unique materials were used.

9. Antibodies

Describe the antibodies used and how they were validated for use in the system under study (i.e. assay and species).	Anti-HA antibody: Thermo Fisher Scientific 26183 IgG antibody control: Sigma I5381 G3BP1 primary antibody: Abnova H00010146-B01P Antibodies were only chosen if there were validated references available.

10. Eukaryotic cell lines

a. State the source of each eukaryotic cell line used.	HEK293FT and A375 cell lines were acquired from ATCC.
b. Describe the method of cell line authentication used.	None of the cell lines used were authenticated
c. Report whether the cell lines were tested for mycoplasma contamination.	Cell lines were not tested for mycoplasma
d. If any of the cell lines used are listed in the database of commonly misidentified cell lines maintained by ICLAC, provide a scientific rationale for their use.	No commonly misidentified cell lines were used.

Animals and human research participants

Policy information about studies involving animals; when reporting animal research, follow the ARRIVE guidelines

11. Description of research animals

Provide details on animals and/or animal-derived materials used in the study.	No animals were used.

Policy information about studies involving human research participants

12. Description of human research participants

Describe the covariate-relevant population characteristics of the human research participants.	The study did not involve human research participants.